A new mutually destabilized reactive hydride system: LiBH$_4$–Mg$_2$NiH$_4$

Nils Bergemann [a], Claudio Pistidda [a,*], Maike Uptmoor [a], Chiara Milanese [b], Antonio Santoru [a], Thomas Emmler [a], Julián Puszkiel [a], Martin Dornheim [a], Thomas Klassen [a,c]

[a] *Department of Nanotechnology, Institute of Materials Research, Helmholtz-Zentrum Geesthacht, 21502, Geesthacht, Germany*
[b] *Pavia Hydrogen Lab, C.S.G.I. and Chemistry Department, Physical Chemistry Section, University of Pavia, 27100 Pavia, Italy*
[c] *Institute of Materials Technology, Helmut-Schmidt-University, 22043 Hamburg, Germany*

ABSTRACT

In this work, the hydrogen sorption properties of the LiBH$_4$–Mg$_2$NiH$_4$ composite system with the molar ratio 2:2.5 were thoroughly investigated as a function of the applied temperature and hydrogen pressure. To the best of our knowledge, it has been possible to prove experimentally the mutual destabilization between LiBH$_4$ and Mg$_2$NiH$_4$. A detailed account of the kinetic and thermodynamic features of the dehydrogenation process is reported here.

© 2019 Science Press and Dalian Institute of Chemical Physics, Chinese Academy of Sciences. Published by Elsevier B.V. and Science Press. All rights reserved.

1. Introduction

In the last decades, the hydrogen absorption and desorption properties of complex metal hydrides such as borohydrides [1,2], amides [3] and alanates [4] have been extensively investigated, due to their high gravimetric hydrogen storage capacity [5,6]. However, the reaction enthalpies of the complex metal hydrides are usually too high for most applications. In addition, the products of their thermal decomposition are often too stable to allow full reversibility under moderate temperature and hydrogen pressure conditions. To modify the stability of complex metal hydrides, several approaches can be followed. For example, the partial cation substitution by elements with higher Pauling electronegativity was shown to reduce the enthalpy change upon dehydrogenation and therefore the desorption temperature [7–9]. Another effective approach was developed based on the work performed in 1967 by Reilly and Wiswall [10] and applied to borohydrides. In this approach, it was shown that the stability of a borohydride could be lowered by combining it with a suitable reaction partner (i.e. metals such as aluminium, magnesium or titanium) [11–14]. A major disadvantage of this approach is the considerable reduction of gravimetric hydrogen storage capacity due to the additional weight

of the metal. The use of an appropriate hydride instead of the pure metal from one hand enables maintaining a high hydrogen storage capacity and from the other hand leads to the formation of fully reversible systems under moderate temperature and hydrogen pressure conditions. Such systems are called Reactive Hydride Composites (RHC).

Reactive Hydride Composite systems are not necessarily based on borohydrides. In fact, one of the first reported RHC was the LiNH$_2$–LiH system [15] and many more followed in the successive years. Nevertheless, especially for borohydrides, the RHC approach attracted a lot of attention, in particular after the encouraging experimental results about the LiBH$_4$–MgH$_2$ system published by Barkhordarian et al. [16,17] and Vajo et al. [18]. Upon dehydrogenation of LiBH$_4$–MgH$_2$, boron is transferred to magnesium and MgB$_2$ is formed:

$$2LiBH_4 + MgH_2 \rightarrow 2LiH + MgB_2 + 4H_2 \qquad (1)$$
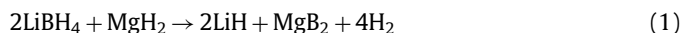
This boron transfer proved to be crucial to allow for relatively mild rehydrogenation conditions and simultaneously preserve the system's storage capacity upon hydrogen cycling. Barkhordarian et al. explained the superior kinetic properties of borohydride formation in systems based on MgB$_2$ by the particular crystal structure of this compound which is composed of alternating magnesium and boron layers [19]. Within each boron layer all atoms are bonded covalently to three other boron atoms. In contrast,

* Corresponding author.
E-mail address: claudio.pistidda@hzg.de (C. Pistidda).

in the typical decomposition products of pure $LiBH_4$, i.e. elemental boron and $Li_2B_{12}H_{12}$, each atom establishes five boron-boron bonds, though. Consequently, the authors attributed the low reactivity of these compounds to high activation barriers associated with breaking the larger number of bonds per atom (i.e. higher binding energy per boron atom). This example shows that in an efficient and reversible RHC not only the dehydrogenation temperatures are effectively lowered but at the same time the reaction products must allow for the reverse reaction in order to achieve high degrees of the reversibility even after many sorption cycles. The $LiBH_4$–MgH_2 (or LiH–MgB_2) system doped with transition metal (TM) based additives typically stores an amount of hydrogen higher than 9 wt% over more than 20 full hydrogenation/dehydrogenation cycles providing a high degree of reversibility [20,21]. However, despite an expected equilibrium temperature of 225 °C at 1 bar H_2 [22], the experimentally determined operational temperatures are typically well above 300 °C. In order to release hydrogen at reasonable rates, temperatures around 400 °C must often be applied. Moreover, it could be demonstrated that the dehydrogenation does not occur in a concerted reaction between $LiBH_4$ and MgH_2 [23,24]. Instead, the first reaction step always appears to be the independent decomposition of MgH_2. Hence, the dehydrogenation proceeds via an – in terms of the Gibbs free energy G – activated state, i.e. $LiBH_4$–Mg. In addition, the formation of stable side products must also be considered: if the dehydrogenation pressure is lower than approximately 3 bar H_2, the partial decomposition of $LiBH_4$ into $Li_2B_{12}H_{12}$, LiH and hydrogen is observed.

Aiming at finding a RHC system based on $LiBH_4$ capable to dehydrogenate and rehydrogenate through single step reactions, our attention fell on the $LiBH_4$–Mg_2NiH_4 system. In fact, Mg_2NiH_4 [25–31] stores an amount of hydrogen equal to 3.6 wt% and is less stable than MgH_2. Consequently, it is expected to trigger an operation temperature lower than that observed for the $LiBH_4$–MgH_2 system. The hydrogen absorption and desorption properties of the $LiBH_4$–Mg_2NiH_4 system were already partially investigated by Vajo et al. In their work, they observed the formation of $MgNi_{2.5}B_2$ upon dehydrogenation and the partial recovery of $LiBH_4$ during rehydrogenation [18,32]. In this work, we aim at complementing the results obtained by Vajo et al. through a thorough study of the dehydrogenation and rehydrogenation mechanisms and their dependency on experimental parameters. Special emphasis was put on studying the impact of the applied hydrogen pressure and temperature on the dehydrogenation mechanism. As $LiBH_4$ forms amorphous boron and $Li_2B_{12}H_{12}$ upon dehydrogenation at elevated temperature, an important aspect of this study was to find out whether such side products are also formed in the hydride composite investigated here. Moreover, the stability of the system's storage capacity upon hydrogen cycling, i.e. the reversibilities of the sorption reactions, was also investigated.

2. Experimental

Most chemical compounds used in this work are commercially available and were purchased from different suppliers. To reduce the impact of impurities on the prepared samples, i.e. on their hydrogen storage properties, only highly pure materials were used. A list of the different compounds stating the respective purity and the supplier is provided in Table S1. Mg_2NiH_4 and $MgNi_{2.5}B_2$ are not commercially available and were synthesized in-house following the procedures described here. As many materials utilized in the experiments described below are sensitive to oxygen and/or humidity, they were handled in argon-filled gloveboxes under a continuously purified argon flow (O_2 and H_2O levels ≤ 1 ppm). The RHC systems were prepared using a SPEX SamplePrep 8000 Mill

and hardened steel milling vials. For this purpose, the mixtures were milled for 300 min using a ball-to-powder (BTP) ratio of 10:1.

Since Mg_2NiH_4 is not commercially available, it was synthesized in-house starting from MgH_2 and Ni. The two compounds were mixed in a molar ratio of 2:1 and milled for 4 h in a planetary FRITSCH P6 mill using Al_2O_3 vials and balls. A ball-to-powder ratio of 5:1 was applied and the rotation speed was set to 300 rpm. Subsequently, the mixture was annealed at 400 °C under a hydrogen pressure of 225 bar. As the powdery material already contained all the hydrogen amount required for the formation of Mg_2NiH_4, the pressure value was chosen arbitrarily and solely to prevent any dehydrogenation reaction upon heat treatment. The diffraction patterns of the as-milled and the annealed material are presented in Fig. S1. Mg_2NiH_4 exists in two polymorphic structures. At temperatures below approximately 250 °C the monoclinic modification (space group C12/c1, No. 15) [31] is the thermodynamically stable form. Above that temperature only the cubic polymorph (space group Fm-3m, No. 225) [27] can be found. As it can be seen in Fig. S1, a mixture of both polymorphs was partially formed already upon ball milling. After the heat treatment only minor amounts of the initial reactants are recognized in the diffraction pattern. The Rietveld refinement confirms a purity of approximately 90%. The final material is a mixture of the low- and high-temperature polymorph of Mg_2NiH_4.

Similar to Mg_2NiH_4, also $MgNi_{2.5}B_2$ [33–35] could not be purchased and thus had to be prepared in-house. This compound was synthesized from a mixture of MgB_2 and Ni. The two reactants were combined in a molar ratio of 1:2.5 and subsequently milled for 4 h in a planetary FRITSCH P6 mill employing Al_2O_3 equipment. For this purpose, a ball-to-powder ratio of 5:1 and a rotation speed of 300 rpm were applied. Afterwards, the powder was annealed at 930 °C in argon atmosphere for 24 h. Diffractograms of as-milled and annealed material are shown in Fig. S2(a). The as-milled powder only features the reflections of Ni and MgB_2. However, after the heat treatment, no signals of these two compounds are observed. Instead, only intense reflections of $MgNi_{2.5}B_2$ are identified. The ^{11}B MAS NMR spectra of pure MgB_2 and annealed "$MgB_2 + 2.5Ni$" are presented in Fig. S2(b). It can be seen that the resonance of MgB_2 vanished completely in the latter sample. Only minor quantities of boron containing impurities with resonances between 10 and 20 ppm can be distinguished. Overall, the purity of the as-synthesized $MgNi_{2.5}B_2$ compound, as determined by a Rietveld analysis and the evaluation of the ^{11}B NMR data, reaches a value higher than 95%.

Ex situ powder X-ray diffraction (PXD) measurements were performed using a Bruker D8 Discover diffractometer operating in Bragg–Brentano geometry. The instrument is equipped with a copper K_α source ($\lambda = 1.54184$ Å) and a VÅNTEC-500 area detector from Bruker. The diffractograms were acquired in seven steps in the 2θ range from 10° to 90° (detector centre position) with an acquisition time of 450 s per step. In order to prevent samples from oxidation or hydrolysis, a sample holder equipped with an argon-filled PMMA dome was employed during the measurements. X-rays scattered by this dome are the cause of the broad background distributed around $q \approx 1.5$ Å^{-1} that is present in each diffractogram.

In situ synchrotron radiation powder X-ray diffraction (SR-PXD) experiments were conducted at the synchrotron facility MAX II (beamline I711) at MAX-lab (Lund, Sweden). The X-ray wavelengths were $\lambda \approx 0.99$ Å. An Agilent Titan CCD detector featuring a 2048×2048 pixel array with a pixel size of (60×60) μm^2 was employed. For the acquisition of each two-dimensional diffraction pattern, exposure times of 20 s were used for all experiments. The experiments were performed in Debye-Scherrer geometry with a special in situ diffraction setup that allows for sample temperature and gas pressure recording [36,37]. The specimens were filled into a sapphire capillary (outer diameter 1 mm, inner diameter 0.6 mm)

which was positioned directly in the X-ray beam. This capillary was mounted into the sample holder body with gas tight connections. A thermocouple inserted into the capillary allowed for accurate temperature measurements. A pressure transducer connected to the sample holder was employed to monitor the gas pressure during the in situ experiments. All measurements were conducted in hydrogen atmosphere with a pressure of at least 1 bar. An electrical heating block positioned below the sapphire capillary and operated by a PID controller increased the sample temperature with the desired heating rate to the respective maximum. In order to determine the X-ray wavelength and the instrumental broadening precisely, LaB_6 powder was used. The obtained two-dimensional images were carefully masked to exclude single crystal diffraction spots, e.g. from the sapphire capillary, and then radially integrated to one-dimensional diffractograms by means of the program FIT2D [38,39]. Subsequently, all diffractograms collected in the experiment were combined to a two-dimensional (temperature vs. q-vector) colour-coded intensity map using the software Origin. The program MAUD [40,41] was used to perform Rietveld refinements of ex situ and selected in situ diffractograms. Structural data of the different chemical compounds were included either with Crystallographic Information Files (CIF) taken from the ICSD catalogue or by transferring the crystallographic properties directly from the original publications.

The differential scanning calorimetry (DSC) measurements were carried out in a Netzsch DSC 204 HP heating the samples (about 10 mg each) from room temperature to the respective maximum temperature of the experiment at a rate of 5 K min^{-1}. All measurements were conducted in hydrogen atmosphere with constant pressures of 1, 20 or 50 bar.

The chemical compositions of samples containing nano-crystalline or amorphous phases were determined by solid-state MAS NMR measurements. Spectra of the ^{11}B nucleus were recorded to characterize the distribution of boron within these samples. The measurements were carried out employing a Bruker Avance 400 MHz (128.33 MHz for the ^{11}B nucleus) spectrometer equipped with a wide-bore 9.4 T magnet and a boron-free Bruker CP-MAS probe. The one-dimensional ^{11}B MAS NMR spectra were acquired after a 2.7 μs single $\pi/2$ pulse (corresponding to a radio field strength of 92.6 kHz) and with application of a strong ^1H signal decoupling by using the two-pulse phase modulation (TPPM) scheme. In order to assess quantitatively molar ratios of samples comprising more than one boron containing compound, the areas of resonances and their corresponding spinning sidebands in the range from 1500 to -1500 ppm were considered. For all ^{11}B NMR analysis presented in this work, the chemical shifts were externally referenced to $BF_3 \cdot Et_2O$ and reported in parts per million (ppm). For all measurements the samples were filled into 4 mm ZrO_2 rotors that were closed with Kel-F caps. The packing was done inside argon-filled gloveboxes. The rotors were spun at 12 kHz by applying dry nitrogen gas. During the measurements the sample temperature was kept at 20 °C by Bruker BCU units.

3. Results

In order to assess the sequence of dehydrogenation events of the $LiBH_4$–Mg_2NiH_4 composite, the process was monitored in an in situ SR-PXD experiment. For that purpose, as-milled material was heated from room temperature to 440 °C at a rate of 10 K min^{-1} under 1 bar of hydrogen. As it can be seen in Fig. 1, the as-milled powder features reflections of the low-temperature (lt) polymorph of $LiBH_4$ (space group $Pnma$, No. 62) [42] besides those of the two Mg_2NiH_4 modifications, i.e. the low-temperature monoclinic and the high-temperature (ht) cubic forms are visible. The very first modification of the diffraction patterns occurs at about 111 °C and is associated to the polymorphic transition from lt to ht $LiBH_4$

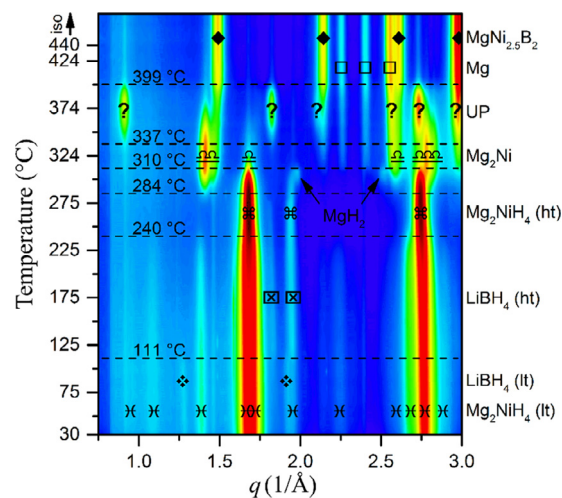**Fig. 1.** In situ SR-PXD analysis of the $LiBH_4$–Mg_2NiH_4 composite: the sample was heated from room temperature to 440 °C at 10 °C min^{-1} in 1 bar of hydrogen.

(space group $P6_3mc$, No. 186) [43]. At roughly 240 °C the transition from Mg_2NiH_4 (lt) to the high-temperature polymorph can be observed. The first chemical reaction occurs at approximately 284 °C as Mg_2Ni is formed. Shortly after, the reflections of $MgNi_{2.5}B_2$ and MgH_2 can be detected as well. The latter are only present for a very short time and disappear at a temperature of approximately 310 °C. Simultaneously, the diffraction pattern of Mg becomes visible. At about 337 °C the reflections of a yet unknown phase arise and intensify. Hereafter this unknown phase is uniformly denoted as UP. At nearly the same temperature, the diffraction intensity of Mg_2Ni starts to decrease. At slightly higher temperatures also the reflections of UP weaken and above approximately 400 °C these two compounds cannot be identified any more. At the end of the experiment, i.e. after a short dwelling time of 5 min at 440 °C, only reflections of $MgNi_{2.5}B_2$ and Mg remain visible.

The influence of the hydrogen back pressure on the dehydrogenation reactions of the $LiBH_4$–Mg_2NiH_4 system was determined by a set of complementary experiments. First of all, the dependency of the hydrogen evolution from the as-prepared material was monitored as a function of temperature at 1, 5 and 50 bar H_2. The specimens were heated from room temperature to 400 °C at a rate of 5 °C min^{-1}. The three volumetric analysis are presented in Fig. 2(a). By increasing the hydrogen pressure, the dehydrogenation onset temperature shifts from 297 °C to 335 °C and eventually to 385 °C. Unlike the desorption measured at 1 bar that mainly proceeds in one step, the dehydrogenation process at 5 bar features an additional step: an alteration of the gas evolution rate can be perceived at a hydrogen loss of approximately 2 wt%. The determined total hydrogen capacities are similar for the two experiments conducted at 1 and 5 bar and amount to roughly 4.8 wt%. It should be noted that at both these pressures the last 0.4 wt% evolves at a slower rate. At a back pressure of 5 bar the desorption process requires several hours to reach a stable plateau. On the contrary, at 50 bar the dehydrogenation stops after the first step and no further release of gas is recorded up to 400 °C. Hence, at this pressure only 2 wt% of hydrogen evolves altogether.

The sequence of thermal transitions was determined by the set of DSC analysis shown in Fig. 2(b). To ensure a reliable comparison between these results and the observed evolution of hydrogen, the same experimental conditions were applied as for the volumetric analysis. In the temperature range between 50 °C and 400 °C four endothermic thermal events are visible at all applied hydrogen pressures.
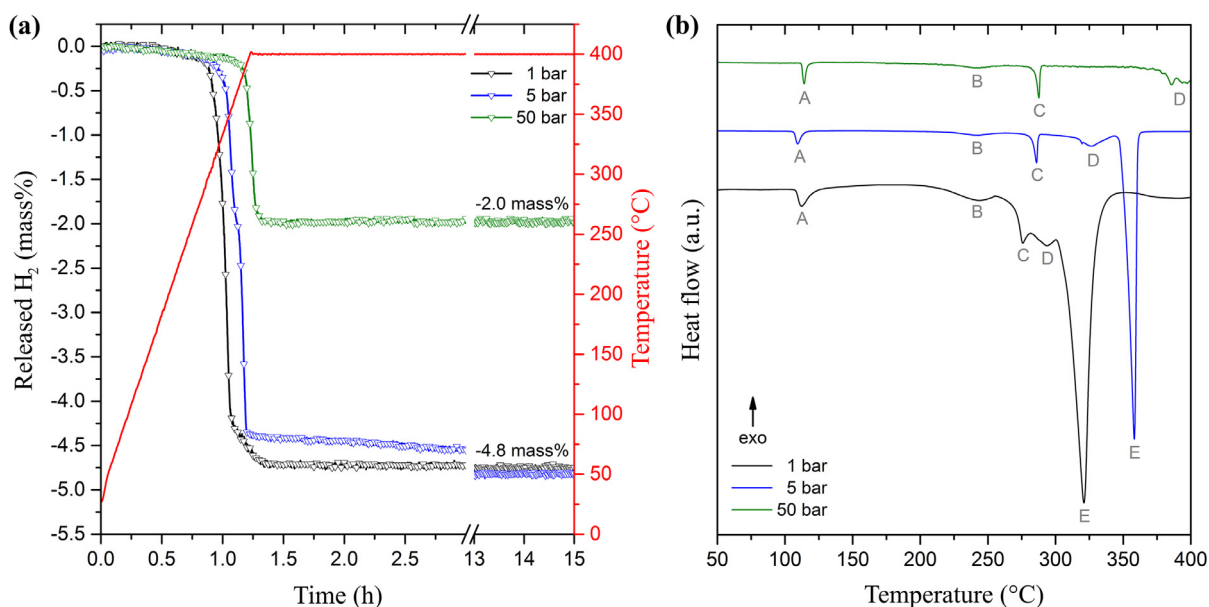
Fig. 2. Dehydrogenation experiments of the $LiBH_4$–Mg_2NiH_4 system conducted at hydrogen pressures of 1, 5 and 50 bar in the temperature range from RT to 400 °C: (a) volumetric analysis and (b) DSC analysis.

The respective peaks are denoted by the letters A to D. In case of the two experiments conducted at 1 and 5 bar, a fifth endothermic event is discernible which is marked with the letter E. The first two transitions are not affected by the applied back pressure. Their onset temperatures are at roughly 110 °C (peak A) and 230 °C (peak B). At 5 and 50 bar H_2, event C also occurs at similar temperatures of about 280 °C. At 1 bar, however, it appears that the onset of this event is slightly shifted to a lower temperature value. Due to the partial overlap of the peaks C and D it is difficult to determine reliable, independent temperatures of these transitions. The onset of the superposition of the two peaks can be estimated at approximately 270 °C. In contrast to the other thermal events the transitions D and E feature an apparent pressure dependence. As just pointed out, at 1 bar H_2 the onset temperature of peak D cannot be determined clearly but should be lower than 280 °C. This temperature rises to 315 °C and eventually to about 375 °C if a back pressure of 5 and 50 bar is applied, respectively. Also, the onset temperature of thermal event E cannot be determined clearly at 1 bar because the respective peak is partially overlapping with peak D. Nevertheless, this temperature is apparently lower than 300 °C and it increases to roughly 345 °C if the pressure is raised to 5 bar.

The chemical composition of the three samples after dehydrogenation was investigated by ex situ PXD and ^{11}B MAS NMR analysis (Fig. 3). As it can be seen in Fig. 3(a), for all hydrogen pressures the most intense X-ray reflections are those of $MgNi_{2.5}B_2$. In addition, all diffractograms contain the patterns of MgH_2. Magnesium can be identified only in the two samples dehydrogenated at 1 and 5 bar.

No reflections of LiH are visible in the diffractogram of the sample desorbed at 1 bar. However, after desorption at the higher pressures the weak (200) reflection can be distinguished. Although the contributions of MgO to the diffraction patterns are not that obvious, Rietveld refinements confirm the presence of small amounts (<5 wt%) among the dehydrogenation products in all three samples. The chemical state of boron is assessed by means of the ^{11}B MAS NMR analysis. The respective three spectra are presented in Fig. 3(b). The distribution of boron atoms in the samples dehydrogenated at 1 and 5 bar is similar: most of the boron atoms are bonded in $MgNi_{2.5}B_2$ (resonance at 154 ppm).

Surprisingly, also a significant amount of MgB_2 (chemical shift 100 ppm) was formed: the molar ratio of boron atoms bonded in $MgNi_{2.5}B_2$ and MgB_2 is roughly 3:1 for both samples. Additionally, a signal at approximately 15 ppm is recorded in case of both these materials. This resonance can be attributed to B-O structures such as $Li_2B_4O_7$ [44,45]. About 5% of the boron atoms are bonded in these impurities. Furthermore, weak signals of residual $LiBH_4$ (chemical shift −41 ppm) are detected. The very low intensity of the $Li_2B_{12}H_{12}$ resonance at −15 ppm indicates a low concentration of this compound after dehydrogenation at 1 bar. At 5 bar this resonance barely stands out against the background. Qualitatively and quantitatively the ^{11}B MAS NMR spectrum of the material desorbed at 50 bar differs significantly from the other two. About 66% of the boron atoms are still bonded in $LiBH_4$ and only 30% were transferred to $MgNi_{2.5}B_2$. Moreover, no traces of MgB_2 and $Li_2B_{12}H_{12}$ are visible. Some impurities of lithium-boron oxides are also detected among the dehydrogenation products in a similar concentration as for the other two samples. It is noteworthy that the chemical shift, the width and the shape of the $MgNi_{2.5}B_2$ resonance change remarkably for the different back pressures. At 1 and 5 bar the centerband maxima are at roughly 154 ppm. However, the width of the $MgNi_{2.5}B_2$ resonance after dehydrogenation at 1 bar (FWHM ≈ 59 ppm) is substantially larger than the one after dehydrogenation at 5 bar (FWHM ≈ 27 ppm). In addition, the shapes of these peaks are highly asymmetrical, especially at 1 bar the intensity at frequencies higher than the peak maximum declines slowly. In contrast, the spectrum of the material dehydrogenated at 50 bar features a rather narrow (FWHM ≈ 8 ppm) and almost symmetrical $MgNi_{2.5}B_2$ resonance that can be approximated by a Gaussian-Lorentzian profile. At 146 ppm, its chemical shift also differs significantly from the frequencies measured for the other two samples. Compared to the as-synthesized $MgNi_{2.5}B_2$ that has a symmetrical resonance with a chemical shift of approximately 142 ppm, the NMR spectrum of the material formed upon dehydrogenation at 50 bar shows by far the closest resemblance.

The considerable differences in the ^{11}B resonance signal of $MgNi_{2.5}B_2$ are caused by structural variations of this compound that should to a certain extend also affect its diffraction patterns. Indeed, upon close examination of the three diffractograms in
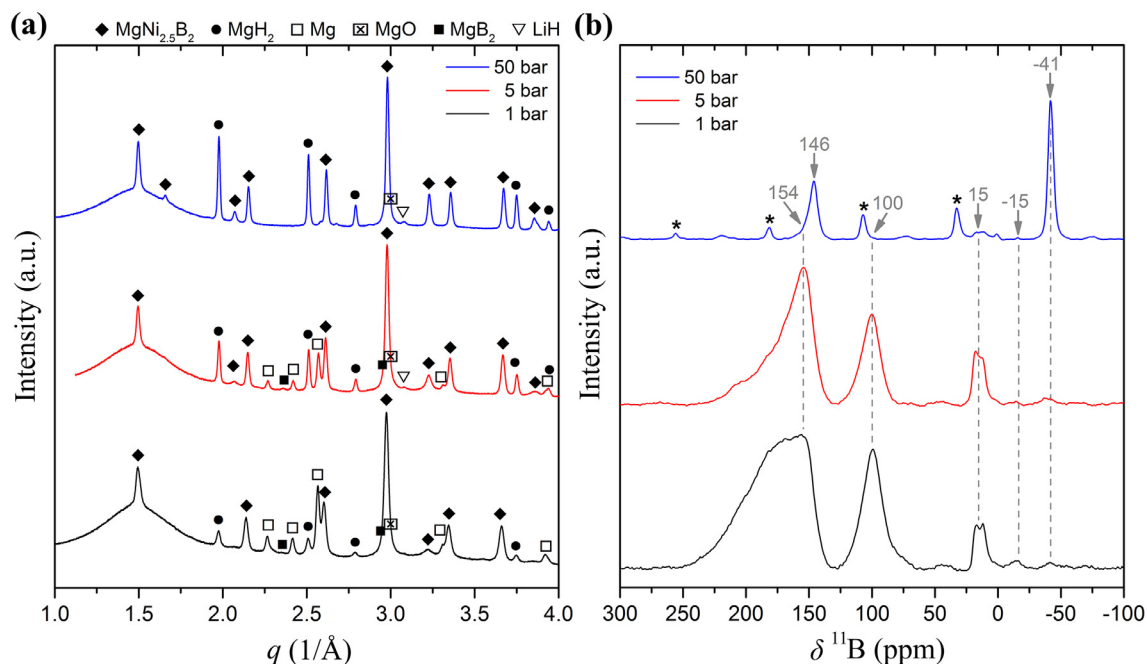
Fig. 3. Determination of the chemical composition of the three $LiBH_4$–Mg_2NiH_4 samples desorbed at hydrogen pressures of 1, 5 and 50 bar (Fig. 2a): (a) PXD analysis and (b) ^{11}B MAS NMR spectra (spinning sidebands are marked with asterisks *).

Fig. 3(a), it is possible to notice alterations in the diffraction pattern of $MgNi_{2.5}B_2$. Besides different peak widths (decreasing with increasing back pressure) also variations in the relative reflection intensities are discernible. In order to quantify these variations and correlate them to changes of the atomic structure of the $MgNi_{2.5}B_2$ crystal, thorough Rietveld refinements of all the three diffractograms in Fig. 3(a) were performed and compared to the respective analysis of as-synthesized $MgNi_{2.5}B_2$. The broad background elevation at about 1.5 $Å^{-1}$ caused by the PMMA dome of the sample holder impeded the preparation of good quality refinements. Therefore, the computation was restricted to the q-range from 1.6 to 5.5 $Å^{-1}$. For illustrative purpose, the final refinement of the diffractogram of the sample dehydrogenated at 5 bar is shown in Fig. 4(a): besides the experimental data, the full refinement and the contributions of the individual compounds are presented as well as the residual plot. The two regions from 2.03 to 2.2 $Å^{-1}$ and from 3.15 to 3.4 $Å^{-1}$ are highlighted because they contain each one pair of $MgNi_{2.5}B_2$ reflections ((102)/(003) and (104)/(113)) that visualize well the variations in the relative peak intensities for the different dehydrogenation pressures. Both regions are shown enlarged in Fig. 4(b). With respect to their neighbouring reflections, the intensities of the (102) and (104) peaks decrease when decreasing the hydrogen pressure. Furthermore, among the three diffractograms a systematic shift of the $MgNi_{2.5}B_2$ reflections (the lower the pressure, the lower the Bragg angles) becomes evident in the expanded view.

If the as-synthesized $MgNi_{2.5}B_2$ is regarded as a reference, the corresponding diffraction pattern of this compound obtained upon dehydrogenation of $LiBH_4$–Mg_2NiH_4 at 50 bar clearly shows the closest resemblance. This qualitative observation is supported by the quantitative Rietveld analysis. For the refinements of the diffratograms of the three desorbed samples, the $MgNi_{2.5}B_2$, MgH_2, LiH and MgO phases were considered. For 1 and 5 bar, Mg and, as suggested by the NMR analysis, MgB_2 were additionally taken into account. The inclusion of the latter compound certainly improves the refinements. For instance, without the contribution of the MgB_2 (101) reflection the calculated intensity of the $MgNi_{2.5}B_2$ (200) reflection (at approximately 3 $Å^{-1}$) is too low to perfectly

match the experimental diffraction intensity. In case of the diffraction pattern of the reference material (as-synthesized $MgNi_{2.5}B_2$), only the crystal structures of $MgNi_{2.5}B_2$ and MgO were considered in the refinement process. In order to reach suitable starting parameters for the refinements of the $MgNi_{2.5}B_2$ crystal structure, initially only the crucial parameters were optimized, i.e. the background, the sample displacement, the phase fractions, the cell parameters, the microstructures and the thermal factors. Once the fit could not be improved any further with the given set of free parameters, also the atomic parameters of $MgNi_{2.5}B_2$ (atom positions and site occupancies) were refined. For that purpose, the initial atomic configuration was specified according to the ideal values of this crystal structure: all occupancies were set to 1 and all atoms were restricted to their specific sites, i.e. Ni atoms on sites 6*f* and 3*d*, Mg atoms on site 3*a* and boron atoms on site 6*i*. Since the possible substitution of Ni by Mg atoms as described by Jung [34] was not taken into account in the refinement process, the scattering capabilities of the atomic sites were solely adjusted by their total occupancies and thermal factors. Initial values for the general atomic coordinates, i.e. those coordinates did not coincide with symmetry elements of the space group, were taken from the structure reported by Jung [34]. In fact, most atomic coordinates in the $MgNi_{2.5}B_2$ crystal are special positions, i.e. they correspond to the space group's symmetry elements. Only the *z*-coordinate of site 6*f* (Ni) and the *x*- and *y*-coordinates of site 6*i* (boron) are general positions. Due to the low sensitivity of the Rietveld refinement to parameters related to the boron atoms (weak atomic scattering factor) and the limitations of the experimental data, the parameters of site 6*i* could not be refined rigorously. Instead, the atomic coordinates were fixed to the literature values and solely the total occupancy as well as the thermal factor of this site were refined. The crucial parameters of the Rietveld analyses are summarized in Table 1. The reference material has the smallest cell parameters and consequently the lowest cell volume of 181.57 $Å^3$. In addition, all site occupancies were calculated to be 1 yielding an atomic ratio of Mg:Ni:B = 1:3:2. With respect to this reference material the cell parameters of the $MgNi_{2.5}B_2$ crystals formed upon desorption of $LiBH_4$–Mg_2NiH_4 are enlarged. At cell volumes
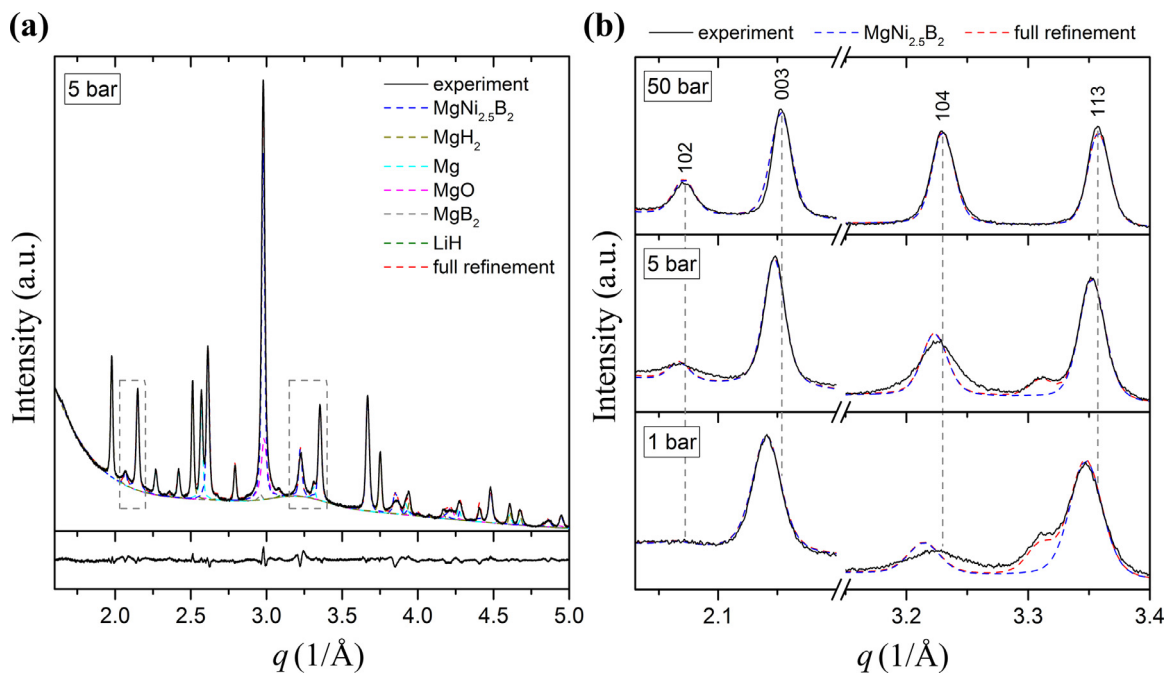
Fig. 4. Rietveld refinements of the PXD analysis of the three dehydrogenated LiBH$_4$–Mg$_2$NiH$_4$ samples presented in Fig. 3(a): (a) full refinement of the sample desorbed at 5 bar for the q-range from 1.6 to 5.5 Å^{-1} and (b) detailed view on the two regions from 2.03 to 2.2 Å^{-1} and from 3.15 to 3.4 Å^{-1} to illustrate the modifications of the relative reflection intensities of MgNi$_{2.5}$B$_2$ for the different dehydrogenation pressures.

Table 1. Refined parameters of the MgNi$_{2.5}$B$_2$ crystal for the three LiBH$_4$–Mg$_2$NiH$_4$ samples desorbed at different hydrogen pressures (Fig. 3a) and for the reference material (Fig. S2a): cell and atomic parameters were determined directly in the refinement. Atomic ratios are based on calculated occupancies. Discrepancy indices are given in form of weighted profile R-factors (R_{wp}) and background subtracted R-factors ($R_{wp,bs}$).[a]

| | Cell parameters | | Atomic parameters | | | | | |
| | | | site 6f | | site 3d | site 6i | Atomic ratio | |
p_{des} (bar)	a (Å)	c (Å)	z	occ.	occ.	occ.	Mg:Ni:B	$R_{wp}/R_{wp,bs}$ (%)
1	4.892	8.847	0.187	0.87	0.81	0.88	1:2.55:1.76	2.5/10.3
5	4.889	8.816	0.197	0.92	0.91	0.63	1:2.75:1.26	2.3/9.8
50	4.886	8.798	0.206	0.99	1.00	0.53	1:2.98:1.06	1.7/6.4
ref.	4.883	8.793	0.207	1.00	1.00	1.00	1:3:2	2.8/9.8

[a] The calculated occupancy of site 3a is 1 for all materials. Values related to boron atoms are subject to a relatively high degree of uncertainty.

of 183.36 Å^3 at 1 bar, 182.49 Å^3 at 5 bar and 181.90 Å^3 at 50 bar, the unit cell expanded approximately 0.99%, 0.51% and 0.18%, respectively, as compared to the as-synthesized MgNi$_{2.5}$B$_2$. This volume expansion, however, is mainly caused by a growth of the cell in z-direction: although the cell parameter c increases by up to 0.61%, the cell parameter a expands only by maximum 0.18%. Also the atomic parameters of the Ni atoms (sites 6f and 3d) show a similar behavior: the lower the dehydrogenation pressure, the larger the discrepancy from the reference values. The calculated occupancies of site 3a (Mg) are 1 for all materials. Only the parameters of the boron atoms (site 6i) follow a different pattern. Here the highest occupancy was calculated for the structure formed at 1 bar. Instead, at 50 bar a site occupancy of only 0.53 was determined. Due to the low influence of boron on the diffraction patterns of MgNi$_{2.5}$B$_2$ and the fixation of the atomic coordinates of site 6i, the given occupancies of this site should be treated with care. Altogether, the resemblance to the as-synthesized material increases with increasing dehydrogenation pressure.

The onset temperature of the reaction associated with the exothermic event D in the DSC analysis conducted at 1 bar (Fig. 2b) is lower than 280 °C and thus lower than the melting temperature of pure LiBH$_4$. This observation hints at the possibility that Mg$_2$NiH$_4$/Mg$_2$Ni also interacts with solid LiBH$_4$ in a reaction that leads to releasing hydrogen. To verify this assumption a

specimen of LiBH$_4$–Mg$_2$NiH$_4$ was heated to 270 °C, i.e. the temperature was kept below the melting point of LiBH$_4$. In addition, a hydrogen pressure of 4 bar was applied to prevent the decomposition of Mg$_2$NiH$_4$. The volumetric analysis of this experiment is shown in Fig. 5(a). A release of gas could be observed already below 200 °C. Although about 2 wt% of hydrogen was released within the first 90 min of the experiment, the reaction kinetics slowed down significantly afterwards. At the end of the experiment, i. e. after a dwell time of 40 h at 270 °C, only approximately 3.3 wt% H$_2$ was released. After cooling the specimen down to room temperature, the consistency and structure of the material was analyzed. It can be described as a homogeneous, fluffy powder with very low mean particle size. No hints of a possible melting of LiBH$_4$ were found. The chemical composition of the sample was determined by means of a PXD analysis (Fig. 5b). Besides the reflections of unreacted Mg$_2$NiH$_4$ and LiBH$_4$ also those of MgNi$_{2.5}$B$_2$ and MgH$_2$ were identified.

The ^{11}B NMR spectrum of the LiBH$_4$–Mg$_2$NiH$_4$ composite dehydrogenated at 1 bar H$_2$ (Fig. 3b) only contains a very weak signal that can be attributed to Li$_2$B$_{12}$H$_{12}$. However, if pure LiBH$_4$ or composites containing this borohydride are heated above 350 °C without sufficient hydrogen back pressure, Li$_2$B$_{12}$H$_{12}$ is usually formed in much higher quantities. In addition, the volumetric analysis conducted at 1 and 5 bar (Fig. 2a) reveal that the last (approximately)
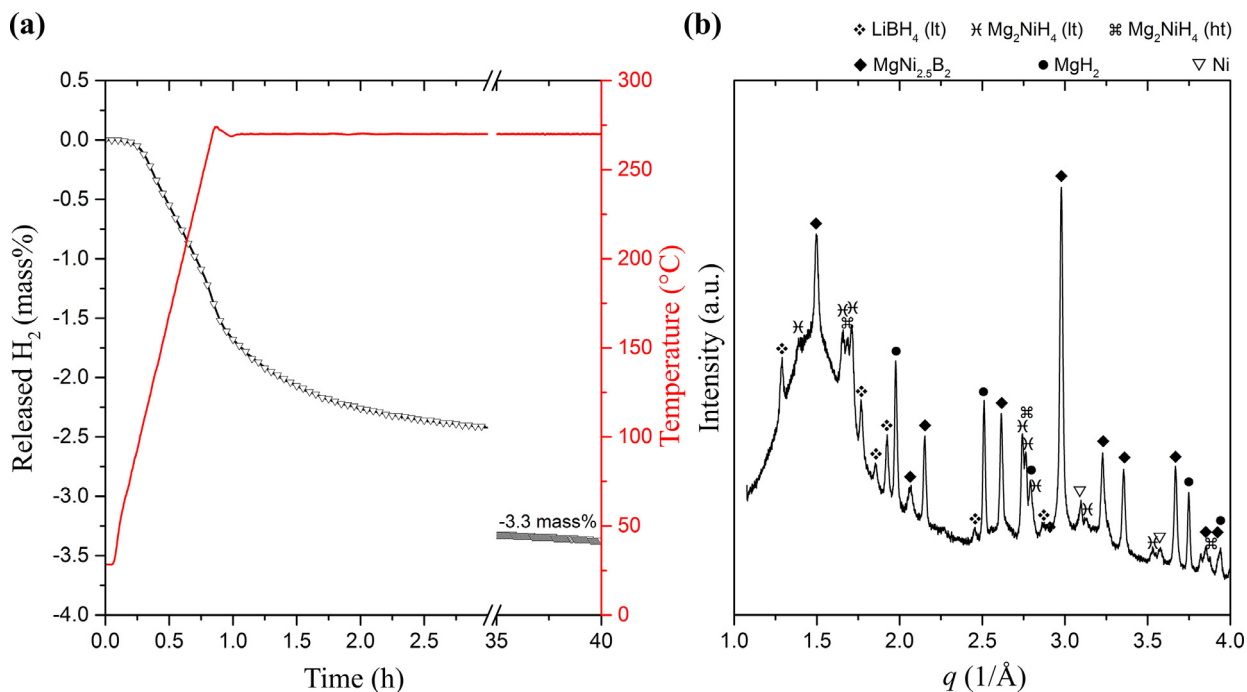
Fig. 5. Dehydrogenation of the $LiBH_4$–Mg_2NiH_4 system at temperatures below the melting point of $LiBH_4$: (a) volumetric analysis conducted at a hydrogen pressure of 4 bar and a maximum temperature of 270° C and (b) PXD analysis of the desorbed sample.
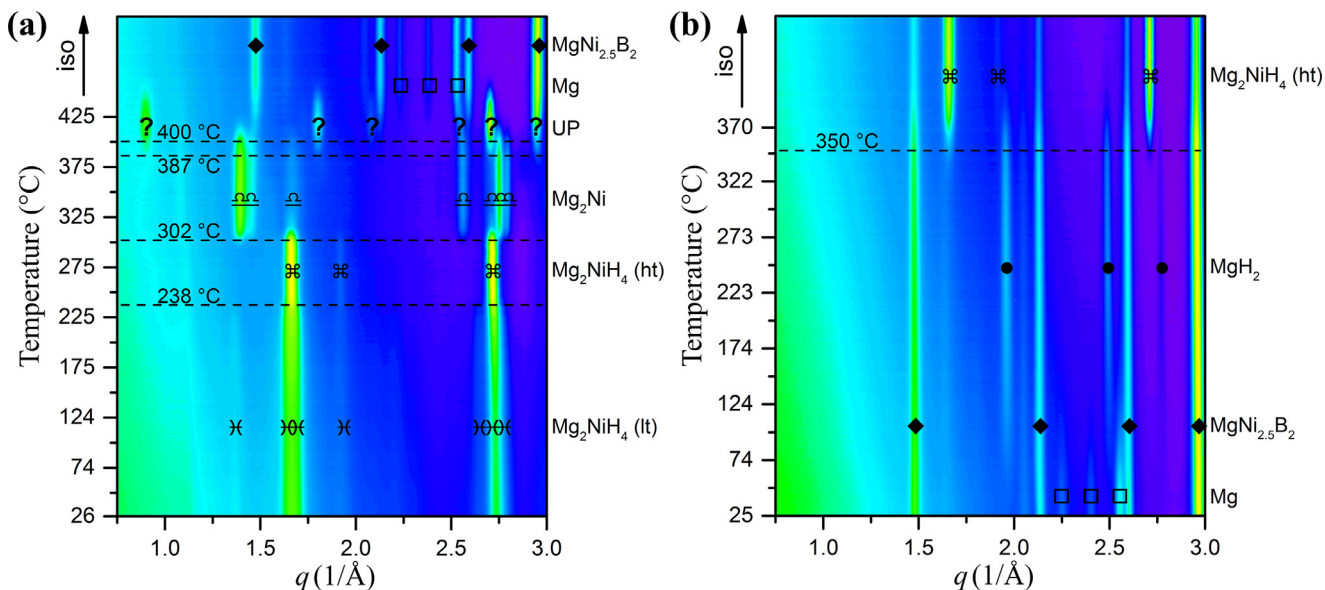

Fig. 6. SR-PXD experiments demonstrating the reactions between Mg_2NiH_4 and $Li_2B_{12}H_{12}$: (a) dehydrogenation at 1 bar and a maximum temperature of 425 °C and (b) subsequent rehydrogenation at 160 bar and a maximum temperature of 370 °C.

0.4 wt% of hydrogen is released at noticeably reduced rates. This observation could be related to reactions involving $Li_2B_{12}H_{12}$. Altogether, it appears reasonable to assume that Mg_2NiH_4/Mg_2Ni could react with $Li_2B_{12}H_{12}$ if this compound occurs during dehydrogenation. Since the processes considered here are intermediate reactions, their study is not possible by means of the ex situ analysis performed after full dehydrogenation of $LiBH_4$–Mg_2NiH_4. Hence, in order to verify the assumption, Mg_2NiH_4, $Li_2B_{12}H_{12}$ and LiH were mixed in a 15:1:10 ratio. This composition theoretically allows for the bonding of all boron in $MgNi_{2.5}B_2$ and $LiBH_4$, respectively. A sample of this material was investigated in an in situ SR-PXD experiment (Fig. 6). First of all, this sample was dehydrogenated at a pressure of 1 bar H_2 by heating it from room temperature to 425 °C

at a rate of 5 °C min^{-1}. After a dwell time of 40 min the sample was cooled down to room temperature. For the subsequent rehydrogenation the hydrogen pressure was raised to 160 bar and the sample temperature was increased to 370 °C at 5 K min^{-1}. After an isothermal heating period of 20 min the experiment was eventually terminated. As can be seen in Fig. 6(a), the diffractogram of as-milled material that was collected at room temperature only exhibits intense reflections of Mg_2NiH_4 (lt and ht). At about 238 °C the polymorphic conversion of this hydride is observed i.e. afterwards solely the reflections of the high-temperature form remain present up to approximately 302 °C. At this temperature Mg_2NiH_4 decomposes and the diffraction pattern of Mg_2Ni arises. At 387 °C the reflections of UP become discernible. Shortly after, at roughly

400 °C, also those of $MgNi_{2.5}B_2$ and Mg emerge. In contrast to the reflections of UP which fade completely in the isothermal period, the diffraction intensities of $MgNi_{2.5}B_2$ and Mg maximize and stabilize in conjunction with the disappearance of UP. Also, after cooling down to room temperature $MgNi_{2.5}B_2$ and Mg remain the only diffractive compounds that are discernible with the given experimental resolution. The consecutive hydrogenation at 160 bar begins with the conversion of Mg into MgH_2 (Fig. 6b). This process starts already at temperatures lower than 75 °C. However, the second hydrogen absorption step only occurs above 350 °C i.e. above the melting temperature of $LiBH_4$. The reflections of cubic Mg_2NiH_4 emerge whilst those of $MgNi_{2.5}B_2$ and MgH_2 weaken. The diffraction peaks of the latter two compounds diminish continuously during isothermal dwell time – MgH_2 almost vanishes. As opposed to this the diffraction pattern of Mg_2NiH_4 intensifies until the termination of the experiment.

With regard to the utilization of hydrogen storage systems for technical applications, the reversibility of the absorption and desorption processes is essential. The agglomeration of inert side products, phase segregation or the development of large, reaction-inhibiting microstructures are phenomena that diminish the system's hydrogen capacity and/or its sorption rates steadily. Thus, it is crucial to investigate such issues in order to adopt appropriate measures to avoid or minimize them. Typically, a first step to carefully characterize the reversibility of a hydrogen storage system is the monitoring of hydrogen release and uptake over several full sorption cycles. Unfortunately, the high absorption pressures of $LiBH_4$–Mg_2NiH_4 prohibit the use of the volumetric apparatuses for these kinds of cycling experiments. Therefore, the cycling of the material had to be performed in a temperature controlled autoclave. As a consequence, the storage capacity could not be recorded for the individual cycles. Instead, nine full desorption-absorption cycles were performed consecutively. For the dehydrogenation periods a temperature of 420 °C and a hydrogen pressure of 5 bar were applied. The nine rehydrogenations were conducted at 360 °C and pressures between 200 and 250 bar. Each of these sorption steps was carried out for at least 15 h. Eventually, the material was removed from the autoclave in the hydrogenated state allowing to monitor the tenth desorption iteration with the volumetric apparatus. In Fig. 7(a) the temperature dependent release of hydrogen is shown for the first and the tenth dehydrogenation. Although the onset of the desorption reactions appears to be shifted to slightly higher temperatures after cycling, the overall kinetics remain almost unchanged. In total the cycled material evolved about 4.3 wt% H_2. In comparison to the as-milled sample (4.8 wt%) there is a reduction of approximately 10%. The chemical composition of the sample after the ninth reabsorption and after the tenth desorption was determined by PXD analysis (Fig. 7b). As can be seen, intense reflections of Mg_2NiH_4 (lt and ht) and $LiBH_4$ dominate the diffraction pattern of the hydrogenated material. However, weak reflections of $MgNi_{2.5}B_2$ and MgO are also visible. The diffractogram of the desorbed sample is composed of the reflections of $MgNi_{2.5}B_2$ and Mg but also a small fraction of MgO can be distinguished. However, no other nickel containing phases are detected, especially no Mg_2Ni.

4. Discussion

The dehydrogenation path of $LiBH_4$–Mg_2NiH_4 strongly depends on the applied experimental conditions, i.e. the hydrogen back-pressure and the temperature. The variation of the hydrogen pressure in the non-isothermal experiments revealed some exceptional properties of this hydride composite. In case of the experiments conducted at 1 bar, a reaction pattern similar to most other hydride composites was discovered: dehydrogenation starts with the decomposition of the least stable hydride, i.e. Mg_2NiH_4. Afterwards,

the reactions between Mg_2Ni and $LiBH_4$ lead to the formation of $MgNi_{2.5}B_2$, MgH_2/Mg (depending on the temperature and hydrogen pressure) and LiH. In addition, the yet unknown Mg-Ni-B phase UP is formed that was identified previously as an intermediate compound during dehydrogenation of the $Ca(BH_4)_2$-Mg_2NiH_4 system [46,47]. Also in $LiBH_4$–Mg_2NiH_4, UP must be considered as an intermediate phase because it reacts completely upon dehydrogenation. In contrast, if the hydrogen pressure is high enough to prevent the independent desorption of Mg_2NiH_4, another reaction path can be observed. The very first dehydrogenation step is identified as a concerted reaction between $LiBH_4$ and Mg_2NiH_4. The evidence for this behaviour is provided by the DSC analysis presented in Fig. 2(b). The peaks in the analysis were denoted with the letters A to E. The first three of them can be clearly attributed to thermal transitions of the individual hydrides: peak A and B are related to the polymorphic changes of $LiBH_4$ (low-temperature orthorhombic to high-temperature hexagonal) [42,48] and Mg_2NiH_4 (low-temperature monoclinic to high-temperature cubic) [26,27], respectively, and peak C to the melting of $LiBH_4$ [49,50]. Also peak E can be identified unambiguously as decomposition of MgH_2 [51,52]. Since the equilibrium temperature of this hydride exceeds 400 °C at a pressure of 50 bar, its decomposition is not observed in the respective DSC analysis. The peaks denoted with the letter D are related to the reactions between $LiBH_4$ and Mg_2NiH_4 or Mg_2Ni. The comparison of the in situ SR-PXD experiment conducted at a pressure of 1 bar (Fig. 1) with the respective DSC analysis shows that at this pressure the dehydrogenation starts with the decomposition of Mg_2NiH_4. Shortly after the appearance of the Mg_2Ni reflections, also those of $MgNi_{2.5}B_2$ and MgH_2 arise. The formation of the latter two compounds also explains the low intensity of peak D in the DSC analysis: the exothermic reactions creating $MgNi_{2.5}B_2$ and MgH_2 partially compensate for the enthalpy that is required for the endothermic desorption of Mg_2NiH_4. However, already at a pressure of 5 bar a significant difference in the dehydrogenation process can be identified. At 315 °C the onset of peak D is lower than the equilibrium temperature of Mg_2NiH_4 (T_{eq}(5 bar) > 320 °C). Consequently, the first dehydrogenation step of the $LiBH_4$–Mg_2NiH_4 composite is a direct reaction between the two hydrides. This becomes even more obvious when evaluating the DSC analysis conducted at 50 bar. At this pressure the decomposition temperature of Mg_2NiH_4 is higher than 440 °C but the onset of peak D is at only 375 °C. Supported by the PXD analysis (Fig. 3a) the chemical equation of this concerted reaction can be depicted as

$$2LiBH_4 + 2.5Mg_2NiH_4 \rightarrow 2LiH + MgNi_{2.5}B_2 + 4MgH_2 + 4H_2 \qquad (2)$$

According to this reaction scheme a hydrogen storage capacity of 2.5 wt% is expected. Upon further temperature increase another 2.5 wt% of hydrogen can be released due to the dehydrogenation of MgH_2 yielding a total system capacity of 5.0 wt%. At 4.8 wt% the experimentally determined amounts of hydrogen evolved during the volumetric analysis performed at 1 and 5 bar H_2 (Fig. 2a) are in good agreement (96%) with this value. It is noteworthy that the enthalpy of reaction (2) is remarkably low. This can be easily seen by the comparison of the areas of the two DSC peaks D and E at a hydrogen pressure of 5 bar. The area of peak D (chemical Eq. (2)) is significantly smaller than the area of peak E (decomposition of MgH_2). To be exact, area D covers only about 18% of area E. However, in both reactions the same amount of hydrogen is released, namely 4 moles per formula unit. Consequently, the enthalpy of reaction (2) can be directly estimated from the ratio of the peak areas and the known enthalpy of MgH_2 (74.4 kJ (mol H_2)$^{-1}$ [52]). At roughly 13 kJ (mol H_2)$^{-1}$ the experimentally determined enthalpy is significantly lower than those of common, reversible hydrides and hydride composites. Considering this low reaction enthalpy, a rehydrogenation of the desorption products would be impossible
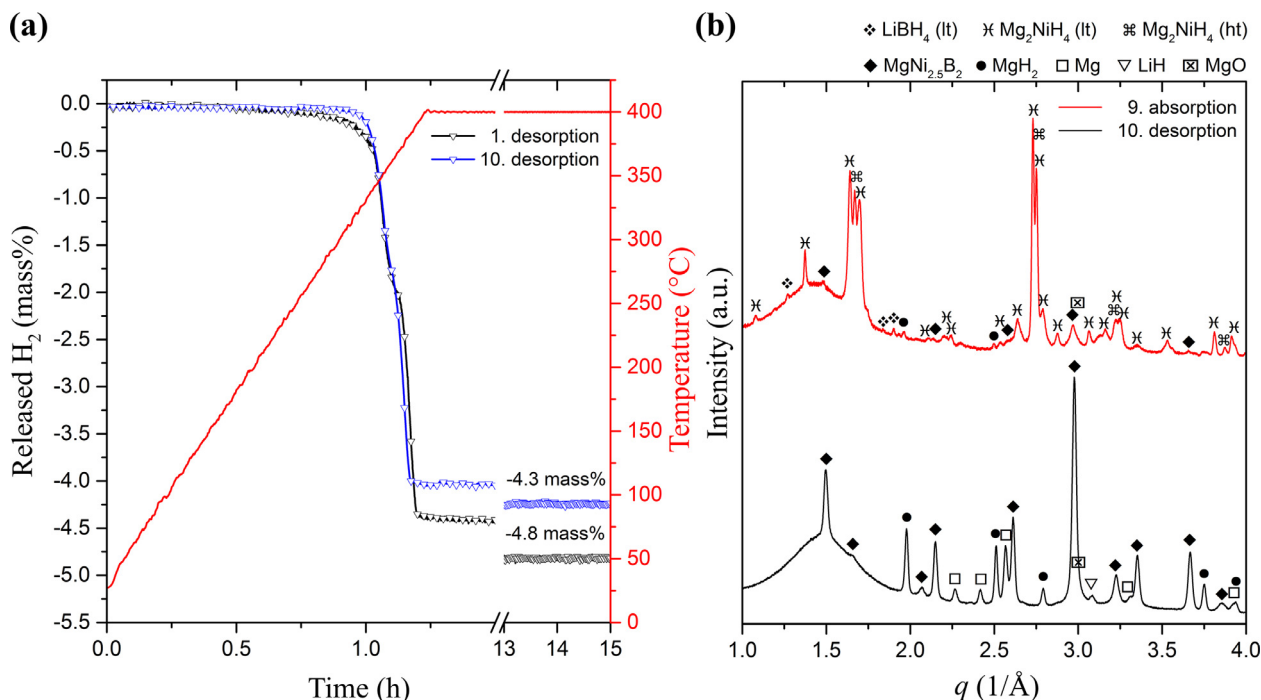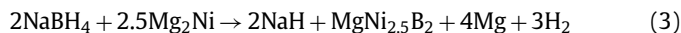
(a)

(b)

Fig. 7. Reversibility of the LiBH$_4$–Mg$_2$NiH$_4$ system upon hydrogen cycling: (a) comparison of the volumetric analysis of the first and tenth dehydrogenation and (b) PXD analysis of cycled material after the ninth rehydrogenation and the tenth dehydrogenation.

at the temperature and pressure conditions employed in the absorption experiments if the entropy change associated with the hydrogenation reaction was similar to those of typical hydrides such as MgH$_2$ or Mg$_2$NiH$_4$ (i.e. ΔS well above 100 J (K mol H$_2$)$^{-1}$) because the equilibrium pressure would be extremely high. Since rehydrogenation was successful at moderate gas pressures, also the entropy change of reaction (2) must be exceptionally low. In fact, Vajo et al. were able to estimate thermodynamic data for the composite LiBH$_4$–Mg$_2$NiH$_4$ by means of a sequence of non-equilibrium measurements [18]. They performed absorption and desorption experiments with varying hydrogen pressures at several constant temperatures and evaluated the rate of the processes. With the assumption that this rate becomes zero if the pressure converges to the equilibrium pressure, the authors could estimate a set of $p_{eq}(T)$ values and construct a van't Hoff diagram. At 15.4 kJ (mol H$_2$)$^{-1}$, the extracted reaction enthalpy is fairly low but in good agreement with the value determined in this work. The entropy change was specified with 62.2 J (K mol H$_2$)$^{-1}$. This value is, as expected, rather low, too. Vajo et al. attributed the low entropy change to the properties of the hydrogenated state. They assumed a comparatively high entropy associated with having the two complex hydride anions [BH$_4$]$^-$ and [NiH$_4$]$^{4-}$. However, this explanation is not satisfactory because the entropy change for the decomposition of pure Mg$_2$NiH$_4$ is reported to be 122.2 J (K mol H$_2$)$^{-1}$ [29]. That is almost the entropy value generated with the release of gaseous hydrogen ($S_{300\,K}$(H$_2$) = 130.77 J (K mol)$^{-1}$, [53]) suggesting that the moderate entropy excess of Mg$_2$NiH$_4$ with respect to Mg$_2$Ni cannot explain the low entropy change of reaction (2). In order to survey the plausibility of the given values, thermodynamic data of several chemical reactions was taken from the literature. Subsequently these reactions were deconstructed and recombined to find estimates for the enthalpy and entropy changes in question. Thermodynamic properties associated with the formation of MgNi$_{2.5}$B$_2$ are not easy to assess because no independent data is reported in the literature. Therefore, the formation of this compound is evaluated with the help of two additional reactions. The first is the one between NaBH$_4$ and Mg$_2$Ni as reported by Afonso et al.:

Table 2. Standard enthalpies of formation ΔH_f^0 and standard molar entropies S^0 of NaBH$_4$, NaH, boron and hydrogen according to the NIST Chemistry WebBook.

Compound	ΔH_f^0 (kJ mol^{-1})	S^0 (J (K mol)$^{-1}$)
NaBH$_4$	−191.8	101.5
NaH	−56.4	40.0
B	0	5.9
H$_2$	0	130.7

$$2\text{NaBH}_4 + 2.5\text{Mg}_2\text{Ni} \rightarrow 2\text{NaH} + \text{MgNi}_{2.5}\text{B}_2 + 4\text{Mg} + 3\text{H}_2 \qquad (3)$$

For this reaction an enthalpy change of 76 kJ (mol H$_2$)$^{-1}$ was measured. The stated value for the entropy change is 113 J (K mol H$_2$)$^{-1}$. The second reaction considered in this context is the decomposition of NaBH$_4$ occurring via:

$$\text{NaBH}_4 \rightarrow \text{NaH} + \text{B} + 3/2\ \text{H}_2 \qquad (4)$$

It should be pointed out that this reaction path is purely hypothetical. In reality, NaH is not stable at the dehydrogenation conditions of NaBH$_4$ which is why the latter compound actually decomposes into liquid Na, boron and hydrogen [54]. Nevertheless, the standard enthalpies of formation ΔH_f^0 and the standard molar entropies S^0 of NaBH$_4$, NaH, boron and hydrogen are listed in the NIST Chemistry WebBook [55] and summarized in Table 2. By means of these values the reaction enthalpy and entropy of chemical Eq. (4) can be calculated to 90.3 kJ (mol H$_2$)$^{-1}$ and 93.8 J (K mol H$_2$)$^{-1}$, respectively.

The combination of reactions (3) and (4) allows to determine the enthalpy and entropy change of the reaction

$$2.5\text{Mg}_2\text{Ni} + 2\text{B} \rightarrow \text{MgNi}_{2.5}\text{B}_2 + 4\text{Mg} \qquad (5)$$
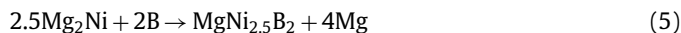
to −42.8 kJ and 57.8 J K^{-1} per formula unit. Furthermore, in order to estimate the thermodynamics of the concerted reaction (2), the decomposition of liquid LiBH$_4$ occurring via the reaction path
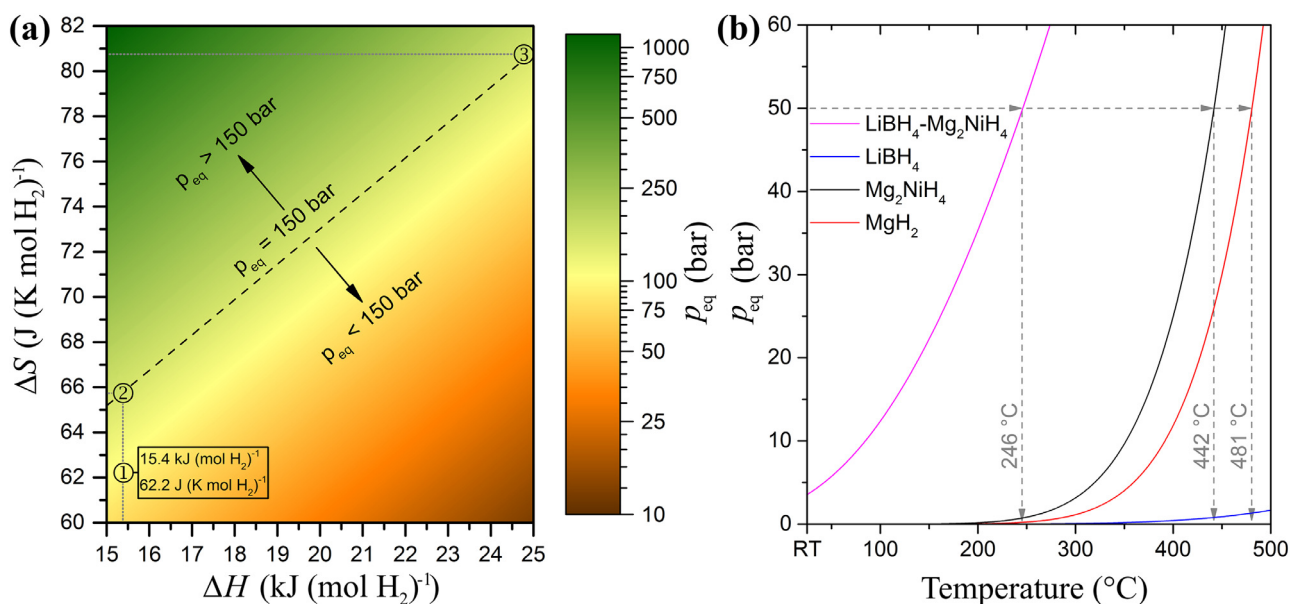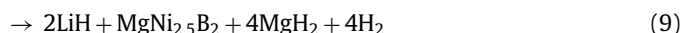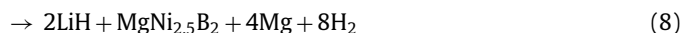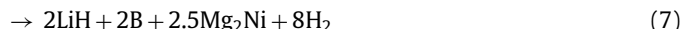
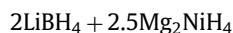$$\text{LiBH}_4\ (\text{liquid}) \rightarrow \text{LiH} + \text{B} + 3/2\text{H}_2 \qquad (6)$$
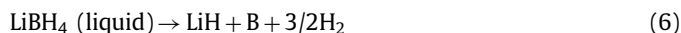
Fig. 8. Assessment of the thermodynamic properties of the $LiBH_4$–Mg_2NiH_4 system: (a) equilibrium pressure of a general absorption process at 365 °C as a function of the reaction enthalpy ΔH and the entropy change ΔS, the plateau pressure of the concerted reaction (2) is located in the lower left part of the diagram (p_{eq}(365 °C) < 150 bar), (b) equilibrium pressures as a function of the temperature for reaction (2) and for the pure compounds $LiBH_4$, Mg_2NiH_4 and MgH_2.

is considered. According to Price et al. the changes of enthalpy and entropy for this reaction are 58.6 kJ $(mol\ H_2)^{-1}$ and 80.1 J (K mol $H_2)^{-1}$, respectively [56]. Whilst taking into account the dehydrogenation paths and the associated enthalpy and entropy changes of pure Mg_2NiH_4 (64.4 kJ $(mol\ H_2)^{-1}$ and 122.2 J (K mol $H_2)^{-1}$, [29]) as well as pure MgH_2 (74.4 kJ $(mol\ H_2)^{-1}$ and 135.1 J (K mol $H_2)^{-1}$, [52]), the combination of reactions (5) and (6) makes it possible to estimate the enthalpy and entropy changes for the dehydrogenation of $LiBH_4$–Mg_2NiH_4. For that purpose, a hypothetical reaction scheme with three individual steps is constructed:

$$2LiBH_4 + 2.5Mg_2NiH_4$$

$$\rightarrow 2LiH + 2B + 2.5Mg_2Ni + 8H_2 \tag{7}$$

$$\rightarrow 2LiH + MgNi_{2.5}B_2 + 4Mg + 8H_2 \tag{8}$$

$$\rightarrow 2LiH + MgNi_{2.5}B_2 + 4MgH_2 + 4H_2 \tag{9}$$

The reaction enthalpies and entropies for the steps (7), (8) and (9) are 62.2 kJ $(mol\ H_2)^{-1}$ and 106.4 (K mol $H_2)^{-1}$, −42.8 kJ and 57.8 J K^{-1} per formula unit and −74.4 kJ $(mol\ H_2)^{-1}$ and −135.1 J (K mol $H_2)^{-1}$, respectively. Consequently, according to the given literature data the overall reaction, i.e. the concerted reaction (2), features an enthalpy change of 39.4 kJ $(mol\ H_2)^{-1}$ and an entropy change of 92.2 J (K mol $H_2)^{-1}$. These values do not support the exceptionally low reaction enthalpies determined in this work and by Vajo et al. Also the extraordinarily low entropy change reported by Vajo et al. is not confirmed.

However, the calculated enthalpy and entropy changes associated with the formation of $MgNi_{2.5}B_2$ are dubious. These calculations rely partially on the data provided by Afonso et al. [57]. On closer examination of their raw data, it is clear that their results are subject to considerable uncertainty. Unfortunately, no other publications on this topic are available that could contribute more trustworthy results. Nevertheless, the close resemblance between the enthalpy values determined for the concerted reaction (2) in this work (about 13 kJ $(mol\ H_2)^{-1}$) and by Vajo et al. (15.4 kJ $(mol\ H_2)^{-1}$) lets the magnitude appear reasonable. In Fig. 8(a) the

equilibrium pressure of a general absorption-desorption process is drawn as a function of the reaction enthalpy and entropy at a temperature of 365 °C. Since rehydrogenation of desorbed $LiBH_4$–Mg_2NiH_4 was successfully performed at 365 °C and a hydrogen pressure of 150 bar, this pressure represents an upper limit for the equilibrium pressure of reaction (2). As can be seen, the reaction enthalpy reported by Vajo et al. demands an entropy change of less than 66 J (K mol $H_2)^{-1}$ (point 2). Even if the true reaction enthalpy exceeded the reported value of 15.4 kJ $(mol\ H_2)^{-1}$ by roughly two thirds, the entropy change still would be restricted to values of less than 81 J (K mol $H_2)^{-1}$ (point 3). Consequently, assuming the enthalpy values determined in this work and by Vajo et al. are in the right magnitude, entropy changes of less than 70 J (K mol $H_2)^{-1}$ are plausible. Unlike the explanation attempt given by Vajo et al., not high entropy of the absorbed state is responsible for the low entropy change but rather the reduced entropy of the desorbed state: in reaction (2) liquid $LiBH_4$, a high-entropy hydride, and Mg_2NiH_4 decompose but only 50% of the hydrogen is released into the gas phase. The other half is stored in the low-entropy hydride MgH_2, effectively reducing the entropy change upon desorption. Substantiated by these inferences, the equilibrium pressure of $LiBH_4$–Mg_2NiH_4 was calculated based on the thermodynamic data reported by Vajo et al. (point 1 in Fig. 8a) and compared to the respective pressures of Mg_2NiH_4, MgH_2 and $LiBH_4$. This is shown in Fig. 8(b). At 50 bar H_2 only the composite material features an equilibrium temperature of less than 400 °C confirming once again that the dehydrogenation process observed in the volumetric and DSC analysis is indeed a concerted reaction. However, it can be seen that the measured dehydrogenation onset of this reaction (about 375 °C) is much higher than the calculated equilibrium temperature of 246 °C. Most likely, this discrepancy must be attributed to poor kinetic properties. This assumption is supported by the non-isothermal experiments conducted at 1 bar (in situ SR-PXD and DSC analysis in Figs. 1 and 2b). Although the calculated equilibrium temperature of the concerted reaction is approximately −25 °C at this pressure, the dehydrogenation process starts with the decomposition of Mg_2NiH_4 only at temperatures above 270 °C. It seems that in these experiments with quickly rising temperature the high activation energy of the mutual re-
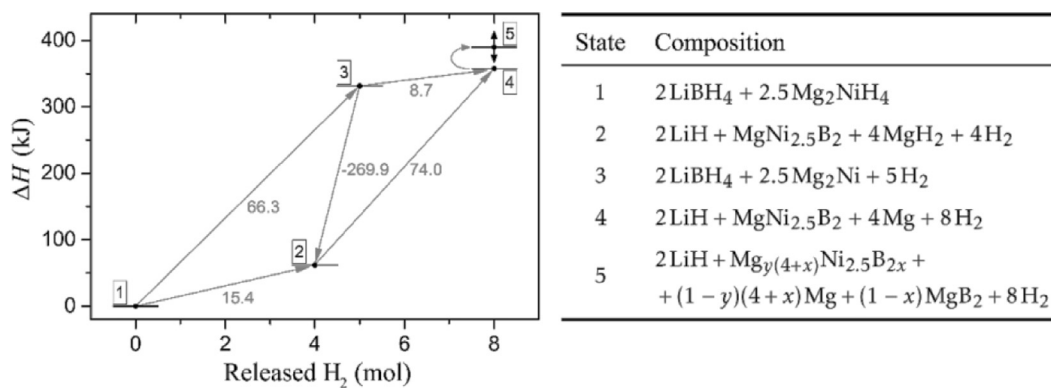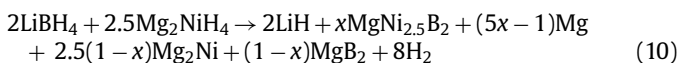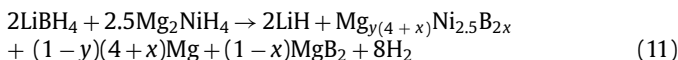
State	Composition
1	$2\,LiBH_4 + 2.5\,Mg_2NiH_4$
2	$2\,LiH + MgNi_{2.5}B_2 + 4\,MgH_2 + 4\,H_2$
3	$2\,LiBH_4 + 2.5\,Mg_2Ni + 5\,H_2$
4	$2\,LiH + MgNi_{2.5}B_2 + 4\,Mg + 8\,H_2$
5	$2\,LiH + Mg_{y(4+x)}Ni_{2.5}B_{2x} +$ $+ (1-y)(4+x)Mg + (1-x)MgB_2 + 8\,H_2$

Fig. 9. Simplified schematic reaction diagram for the LiBH$_4$–Mg$_2$NiH$_4$ RHC: five thermodynamic states are identified (disregarding UP and Li$_2$B$_{12}$H$_{12}$). The grey values at the arrows indicate the reaction enthalpies in kJ (mol H$_2$)$^{-1}$ for the different transitions.

action between LiBH$_4$ and Mg$_2$NiH$_4$ does not allow a discernible reaction rate before the decomposition temperature of Mg$_2$NiH$_4$ is reached. Nevertheless, also at comparatively low temperatures the concerted reaction can be observed, provided the independent decomposition of Mg$_2$NiH$_4$ is inhibited and sufficient time is granted. Even at temperatures below the melting point of LiBH$_4$ the two hydrides effectively destabilize each other. This process is rather unusual because the high kinetic barriers of LiBH$_4$ typically prevent its dehydrogenation in the solid-state. Thus, the discovered behaviour points towards a large driving force (highly negative change of the free energy ΔG) for the mutual reaction which is in agreement with the large deviation between the calculated sorption equilibrium and the measured onset temperature.

After dehydrogenation of LiBH$_4$–Mg$_2$NiH$_4$ at 1 and 5 bar, MgB$_2$ is identified among the desorption products. This compound is formed in the side reaction between Mg and yet unreacted LiBH$_4$. Upon desorption at 50 bar MgH$_2$ is stable and, therefore, no MgB$_2$ is formed. The presence of this compound demands a modification of reaction Scheme (2). If LiBH$_4$ is partially consumed in the side reaction forming MgB$_2$ one would expect to find residual Mg$_2$Ni among the desorption products, i.e. an overall reaction according to

$$2\,LiBH_4 + 2.5\,Mg_2NiH_4 \rightarrow 2\,LiH + x\,MgNi_{2.5}B_2 + (5x-1)Mg$$
$$+ 2.5(1-x)Mg_2Ni + (1-x)MgB_2 + 8\,H_2 \qquad (10)$$

Here $x \in [0.2, 1]$ would be understood as a kinetic parameter describing the amount of produced MgB$_2$. However, no traces of Mg$_2$Ni could be detected in the powder diffractograms. In fact, except for MgNi$_{2.5}$B$_2$, no other Ni-containing compounds are discernible in the PXD analysis (Fig. 3a). In addition, no signals of non-diffractive Ni-B based phases are identified in the NMR spectra (Fig. 3b). Thus, all Ni atoms in these samples must be bonded in MgNi$_{2.5}$B$_2$. Since boron is partially bonded in MgB$_2$, the atomic composition of the Mg-Ni-B compound formed upon dehydrogenation at 1 and 5 bar must differ from the expected ratio of 1:2.5:2. This finding could be explained by a certain homogeneity range of MgNi$_{2.5}$B$_2$, i.e. by a range of atomic compositions with (almost) the same crystal structure (e.g. partial occupancy or atomic substitution). This assumption can also be motivated by the results of the Rietveld analysis (Table 1). Accordingly, the following modified reaction scheme for LiBH$_4$–Mg$_2$NiH$_4$ at 1 and 5 bar can be depicted:

$$2\,LiBH_4 + 2.5\,Mg_2NiH_4 \rightarrow 2\,LiH + Mg_{y(4+x)}Ni_{2.5}B_{2x}$$
$$+ (1-y)(4+x)Mg + (1-x)MgB_2 + 8\,H_2 \qquad (11)$$

The parameter $x \in [0, 1]$ specifies the amount of produced MgB$_2$ but simultaneously determines the ratio of nickel and boron

in MgNi$_{2.5}$B$_2$. Also, in this reaction scheme x can be considered as a kinetic parameter that depends on the experimental conditions such as the hydrogen pressure, the heating rate and the maximum temperature but also on certain properties related to the sample itself like the particle size or the presence of impurities. Hence, it can be assumed that different experimental conditions and sample preparations result in different values for x. The parameter $y \in [0, 1]$ is linked to structural properties of MgNi$_{2.5}$B$_2$. Besides the amount of free magnesium, it describes the ratio of magnesium and nickel within MgNi$_{2.5}$B$_2$ and is, therefore, related to their respective site occupancies and substitutional effects. Based on the chemical compositions of the desorbed samples as determined by the PXD and NMR analysis and supported by the Rietveld refinements of the atomic parameters of MgNi$_{2.5}$B$_2$ (Table 1), the existence of the aforementioned homogeneity range of this compound must be considered the most plausible explanation for the experimental results. Consequently, "MgNi$_{2.5}$B$_2$" should rather be considered a name than an accurate expression of the actual chemical composition of this Mg-Ni-B phase. For convenience, this name is used throughout the whole text in order to refer to this compound.

The temperature and pressure dependent reaction paths and steps can be summarized and visualized in a simplified schematic reaction diagram (disregarding UP and Li$_2$B$_{12}$H$_{12}$) as shown in Fig. 9. The formation enthalpies of the different states are calculated with respect to the fully absorbed state (state 1) that was defined as ground level (0 kJ). The calculations are based on the dehydrogenation enthalpies of Mg$_2$NiH$_4$ and MgH$_2$ reported by Reilly et al. [29] and Stampfer et al. [52], respectively. In addition, the enthalpy change determined by Vajo et al. [18] that is similar to the value measured in this work was assumed for the concerted reaction (2), i.e. the transition from state 1 to state 2. The formation enthalpy of state 5 depends on the parameters x and y and, therefore, is not a fixed value. Since MgNi$_{2.5}$B$_2$ can be synthesized from MgB$_2$ and Ni, this compound must have a more negative standard formation enthalpy (on a per atom basis) as compared to MgB$_2$.

Consequently, state 5 has the highest formation enthalpy among the five states considered in Fig. 9. If LiBH$_4$–Mg$_2$NiH$_4$ is heated up steadily, the reaction path from state 1 to state 2 is thermodynamically the most favourable and should be enabled first. However, high kinetic barriers suppress this path at low temperatures. Hence, at low hydrogen pressures the transition from state 1 to state 3 (decomposition of Mg$_2$NiH$_4$) is observed first. The application of higher hydrogen pressures effectively shifts the sorption equilibrium of Mg$_2$NiH$_4$ to higher temperatures and thus allows for the concerted reaction to take place. State 3 is a non-equilibrium state i.e. the system reacts further immediately. If the temperature is lower than the equilibrium temperature of

MgH$_2$ the gradual transition from state 3 to state 2 is observed. As soon as this temperature is exceeded, the fraction of the system in state 2 quickly passes into state 4. The residual fraction of the system in state 3 reacts gradually to state 4, too. Simultaneously, the newly formed magnesium from state 4 reacts with unreacted LiBH$_4$ from state 3 and forms MgB$_2$. The formation of this compound introduces state 5. This fifth state is thermodynamically less favourable than state 4. However, the presence of MgB$_2$ after full dehydrogenation, i.e. after a dwelling time of several hours at 400 °C, shows that the transition from state 5 to state 4 is kinetically hindered at this temperature.

If LiBH$_4$ or composites containing this borohydride are heated above 350 °C without the application of sufficient hydrogen pressure, the formation of Li$_2$B$_{12}$H$_{12}$ is typically observed. The ^{11}B NMR analysis of dehydrogenated LiBH$_4$–Mg$_2$NiH$_4$ only shows very weak signals that can be attributed to this compound (Fig. 3b). However, it is unlikely that the decomposition of LiBH$_4$ into Li$_2$B$_{12}$H$_{12}$, LiH and hydrogen is somehow suppressed in this composite. Instead, it must be assumed that Li$_2$B$_{12}$H$_{12}$ is partially formed but then acts as a boron donor for Mg$_2$Ni in the formation of MgNi$_{2.5}$B$_2$. The possibility that this reaction occurs under experimental conditions similar to those chosen for the dehydrogenation of LiBH$_4$–Mg$_2$NiH$_4$ was demonstrated in the in situ SR-PXD experiment shown in Fig. 6(a). The composition of the Mg$_2$NiH$_4$-Li$_2$B$_{12}$H$_{12}$-LiH samples was chosen to allow for the bonding of all boron and all nickel in MgNi$_{2.5}$B$_2$. At the end of the dehydrogenation period only MgNi$_{2.5}$B$_2$ but no residual Mg$_2$Ni was detected. Considering the described stoichiometry of the as-prepared material, (almost) full consumption of Li$_2$B$_{12}$H$_{12}$ must be inferred. This experiment also demonstrates the good kinetics for the boron transfer from Li$_2$B$_{12}$H$_{12}$ to MgNi$_{2.5}$B$_2$. Moreover, also in this experiment UP was found to be an intermediate phase. The presence of UP in this sample simultaneously confirms that its formation is not directly associated to LiBH$_4$ but rather to Mg$_2$Ni reacting with any boron donor. Upon rehydrogenation of the desorbed sample Mg$_2$NiH$_4$ was recovered. Its reflections arose at temperatures above the melting point of LiBH$_4$. Therefore, this borohydride was formed in the liquid state making it non-detectable with diffraction methods. Altogether, Li$_2$B$_{12}$H$_{12}$, if produced in a side reaction, must be regarded as an intermediate compound in the LiBH$_4$–Mg$_2$NiH$_4$ system. After complete dehydrogenation all boron is bonded in MgNi$_{2.5}$B$_2$ and thus a full recovery of LiBH$_4$ is possible. This finding is a crucial advantage for the preservation of this system's hydrogen storage capacity and distinguishes it from the LiBH$_4$–MgH$_2$ Reactive Hydride Composite (RHC). As magnesium does not react with Li$_2$B$_{12}$H$_{12}$ under moderate conditions (no formation of MgB$_2$), the latter compound must be regarded as a boron sink in the LiBH$_4$–MgH$_2$ system. The formation of Li$_2$B$_{12}$H$_{12}$ in this RHC causes a gradual degradation of the hydrogen storage capacity as more and more boron is removed from the reversible cycle between LiBH$_4$ and MgB$_2$. In contrast to this, Li$_2$B$_{12}$H$_{12}$ does not constitute a boron sink in the LiBH$_4$–Mg$_2$NiH$_4$ system allowing reversible hydrogen cycling without particular pressure or temperature restrictions.

Due to experimental limitations (the plateau pressure at the hydrogenation temperature exceeds the maximum operation pressure of the volumetric apparatuses), the reversibility of the LiBH$_4$–Mg$_2$NiH$_4$ system could not be recorded continuously over several hydrogen cycles. Instead, the cycling stability had to be evaluated based on ex situ measurements (Fig. 7). The comparison of the volumetric analysis of the first and the tenth dehydrogenation revealed that the reaction kinetics remained almost unchanged. To some extend this observation allows to draw conclusions about the stability of the composite's microstructure. Typically, the development of a refined particle size distribution promotes reaction kinetics. In contrast, a noticeably particle growth causes the opposite i.e. it impedes fast sorption rates. Therefore, no significant

microstructural changes are expected as a result of cycling procedure. However, a drop of the hydrogen capacity of about 10% could be observed. Although this reduction can be partially explained by the presence of MgO – those points towards an exposure to oxygen or humidity during the handling of the material – the low concentration of this impurity suggests that the partial oxidation cannot be held liable for the entire capacity drop. The presence of residual MgNi$_{2.5}$B$_2$ in the hydrogenated state (9. absorption) shows that LiBH$_4$ was not recovered completely during hydrogenation. This finding could be ascribed to several phenomena. For instance, absorption kinetics could reduce sensibly towards the end of the hydrogenation reactions. Such a process could be induced by e.g. the development of new structures and interfaces that impede solid-state diffusion.

Another explanation attempt for the incomplete recovery of the absorbed state could be related to phase segregation which can be motivated by the presence of a liquid phase (LiBH$_4$) in both the absorption and desorption periods. Under the influence of gravity, local deviations from the stoichiometric composition of the LiBH$_4$–Mg$_2$NiH$_4$ composite could develop. Nevertheless, without further detailed characterizations by means of more dedicated techniques the observed capacity drop cannot be explained unambiguously.

Interestingly, the achieved degree of reversibility after ten cycles (about 90%) is much higher than the one obtained by Li and Vajo et al. [32]. In their publication, the authors report a boron transfer to LiBH$_4$ that is equivalent to an absorption yield of only approximately 65%. This rather low value was obtained already for the first three hydrogenation steps. In contrast to the absorption conditions chosen in this work (360 °C, 200 to 250 bar), their hydrogenations experiments were conducted at less absorption-promoting conditions of 160 bar and 350 °C. Considering that the working conditions (temperature, pressure and time) and the material properties (no additives, no compaction) were not optimized for the experiments presented in this work, a reversible capacity of 90% of the starting value after ten full hydrogen cycles must be regarded as good result.

The presented results also provide some insights into the nature of MgNi$_{2.5}$B$_2$. The crystal structure of this compound was characterized for the first time by Jung in 1977 [34]. He described this ternary boride as hexagonal crystal with the space group $P6_2 22$ (No. 180). An illustration of the MgNi$_{2.5}$B$_2$ crystal is presented in Fig. 10. Ni atoms are located at the Wyckoff sites 6f and 3d, most of the Mg atoms at 3a and the B atoms at site 6i. However, about one quarter of the Mg atoms occupies as well 6f and 3d sites. Therefore, these sites are partially occupied by both Ni and Mg; the total occupancies are yet only 89% (3d) and 93% (6f). These crystal structure parameters are summarized in Table 3. In addition, Jung pointed out that single phase diffractograms can also be obtained for slightly different atomic compositions indicating that MgNi$_{2.5}$B$_2$ features a certain homogeneity range as expressed above.

Since the measured cell parameters are practically independent from these changes of the atomic composition, Jung explained his results by modifications of the total and partial occupancies of the Wyckoff sites. This assumption is supported by a publication of Gross et al. from 1998 [33]. The authors reported the crystal structure of MgNi$_3$B$_2$ (Table 3). This compound has similar cell parameters and the same space group as Jung's structure. In contrast to the latter, MgNi$_3$B$_2$ exhibits no substitution of Ni by Mg on the 6f and 3d sites. Moreover, all sites are fully occupied. The authors used a different synthesis method as compared to Jung. Hence, it seems that the structure and atomic composition of MgNi$_{2.5}$B$_2$ (i.e. the site occupancies and the distribution of atoms) are not fixed but depend on the way this compound is formed. With respect to the structural variations of this compound that develop upon dehydrogenation of LiBH$_4$–Mg$_2$NiH$_4$ at different hydrogen pressures, the Rietveld analysis (Table 1) provides a couple of interesting find-
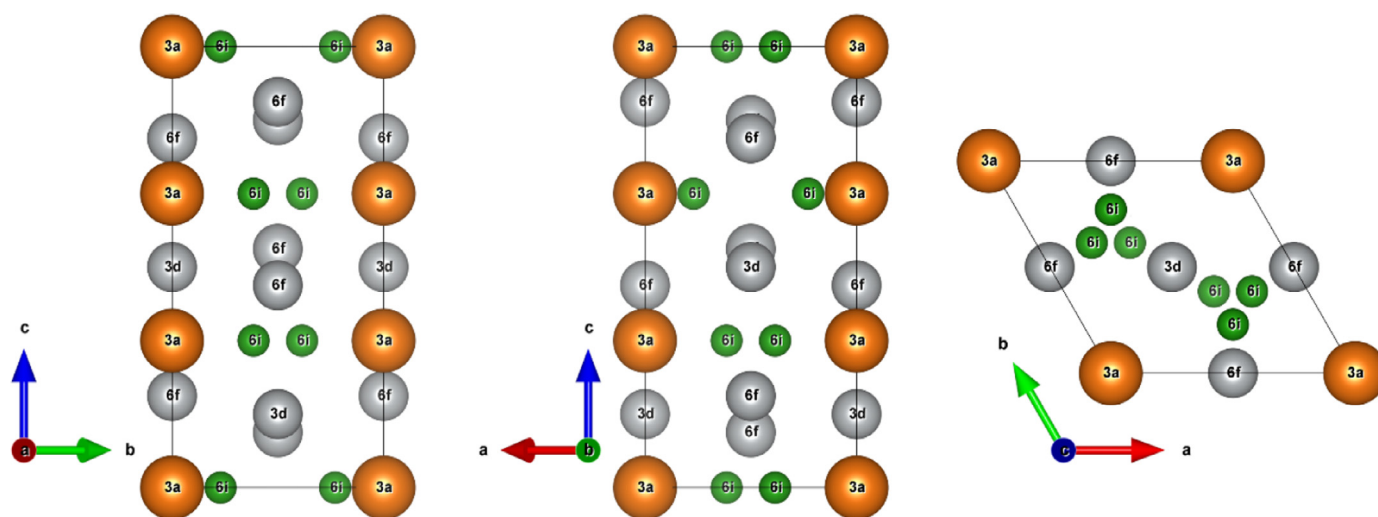
Fig. 10. The crystal structure of MgNi$_{2.5}$B$_2$ viewed along the three crystallographic axes. Nickel, magnesium and boron atoms are portrayed as orange, grey and green spheres, respectively.

Table 3. Crystallographic parameters, i.e. cell lengths a and c, atomic positions x, y and z and site occupancies n, of MgNi$_{2.5}$B$_2$ as reported by Jung and MgNi$_3$B$_2$ as reported by Gross et al.

| | MgNi$_{2.5}$B$_2$, Jung [34] ($a = 4.887$ Å, $c = 8.789$ Å) | | | | | | MgNi$_3$B$_2$, Gross et al. [33] ($a = 4.880$ Å, $c = 8.786$ Å) | | | | | |
| | | | | n | | | | | | n | | |
Site	x	y	z	Ni	Mg	B	x	y	z	Ni	Mg	B
6f	1/2	0	0.208	4.98	0.59	0	1/2	0	0.208	6	0	0
3d	1/2	0	1/2	2.54	0.13	0	1/2	0	1/2	3	0	0
3a	0	0	0	0	2.27	0	0	0	0	0	3.01	0
6i	0.393	0.786	0	0	0	6	0.385	0.771	0	0	0	6

ings. Due to the presence of several diffractive phases, the uneven background functions (scattering at PMMA dome) and the limited resolution of the laboratory diffractometer, some constraints for the interpretation of these results must be considered, though. First, the refinement of the general coordinates of site 6i (boron) had to be omitted because the attempted simultaneous optimization of all atomic parameters of this site led to dubious results. As a consequence, a particular degree of uncertainty for the calculated properties of the boron atoms must be taken into account. Furthermore, the possible substitution of nickel and magnesium on the sites 6f and 3d was not considered in the refinements. Instead, the scattering capabilities of these Wyckoff sites were solely adjusted by their total occupancies and their thermal factors. Consequently, the calculated occupancy values should rather be regarded as measures for the scattering capabilities of these two atomic sites. For instance, a partial replacement of nickel by magnesium atoms on site 3d would lower this site's mean atomic scattering factor $\langle f_{3d} \rangle$ and thus demand a larger total occupancy to produce a similar scattering capability. However, since all Rietveld refinements were conducted in a uniform manner, the presented results are consistent and – within the mentioned limitations – trends between the different samples can be directly concluded. The high quality of the fits, i.e. the low reliability indices in conjunction with the qualitative (visual) assessment of the calculated fit curves, provides a high degree of credibility for the refined cell lengths and atomic parameters of the nickel and magnesium atoms. The following obvious trends for the development of the MgNi$_{2.5}$B$_2$ crystal structure upon dehydrogenation of LiBH$_4$–Mg$_2$NiH$_4$ can be summarized. The lower the applied hydrogen pressure: (1) the larger the unit cell (expansion mainly in c-direction), (2) the smaller the z-coordinate of site 6f (up to −2% of cell length c) and (3) the lower the scattering capabilities of sites 6f and 3d.

It appears plausible to relate these three trends to a more and more disordered crystalline structure. This assumption is also supported by the increased broadening of the MgNi$_{2.5}$B$_2$ reflections perceived after desorption of LiBH$_4$–Mg$_2$NiH$_4$ at lower hydrogen pressures. This broadening is directly related to a reduced mean crystallite size and increased microstrain. The dimensions of the unit cell and the atomic positions are determined by the overall potential created by all atoms in the crystal. Modifications of the atomic site properties (occupancies, substitutional effects) directly affect this potential and thus the energetically best configuration of the crystal. Therefore, it is reasonable to ascribe not only the reduced scattering capabilities of sites 6f and 3d to lowered site occupancies and possible substitutions of nickel and magnesium atoms but also the systematic expansion of the unit cell as well as the shift of the z-coordinate of site 6f. Initially, these occupancy variations and substitutional effects were motivated by the evaluation of the composition of the dehydrogenated LiBH$_4$–Mg$_2$NiH$_4$ samples (reaction Schemes (10) and (11)) but also the Rietveld analysis support this conclusion. In addition, Jung referred to these effects to best describe the MgNi$_{2.5}$B$_2$ diffraction patterns he collected [34]. This line of argument is further substantiated by considering the similar effective ionic radii of Ni^{2+} and Mg^{2+} of 69 pm and 72 pm [58], respectively, which make the possible substitution of these two atoms appear quite plausible. However, for a more detailed evaluation of the MgNi$_{2.5}$B$_2$ crystal structure that develops upon dehydrogenation LiBH$_4$–Mg$_2$NiH$_4$ more and better resolved experimenta data is required. Especially a combination of synchrotron and neutron diffraction analysis could be highly beneficial for this purpose.

The portrayed variations in the MgNi$_{2.5}$B$_2$ crystal structure can be correlated directly to the dehydrogenation pressure and thus to the reaction path of LiBH$_4$–Mg$_2$NiH$_4$. At 1 bar H$_2$ the dehy-

drogenation starts with the decomposition of Mg_2NiH_4. Consequently, $MgNi_{2.5}B_2$ is formed in the reaction between $LiBH_4$ and Mg_2Ni. In addition, the unknown phase UP is produced as an intermediate compound that, upon further reaction, also contributes to the $MgNi_{2.5}B_2$ formation. In contrast, at a hydrogen pressure of 50 bar $MgNi_{2.5}B_2$ is formed exclusively in the concerted reaction between $LiBH_4$ and Mg_2NiH_4. Obviously, this particular reaction path leads to the more ordered structure of the $MgNi_{2.5}B_2$ crystal that bears a much closer resemblance to the structure of the as-synthesized material (Fig. S2) and the ideal configuration of this crystal ($MgNi_3B_2$ structure described by Gross et al. [33]). At 5 bar H_2 the dehydrogenation begins with the concerted reaction between $LiBH_4$ and Mg_2NiH_4. However, at this pressure the equilibrium temperature of Mg_2NiH_4 is lower than 400 °C and thus exceeded upon further heating. Afterwards, the formation of $MgNi_{2.5}B_2$ continues with the consumption of Mg_2Ni and, moreover, involves UP. Consequently, the appearance of $MgNi_{2.5}B_2$ after desorption of $LiBH_4$–Mg_2NiH_4 at 5 bar is a mixture of the ordered structure obtained at higher hydrogen pressures and the disordered one formed at lower pressures. The differences between the reactions of $LiBH_4$ with Mg_2NiH_4 and Mg_2Ni, respectively, might be related to different atomic mobilities at the interfaces of these compounds. The crystal structure of the as-synthesized $MgNi_{2.5}B_2$ also appears well ordered. In this case, the high annealing temperature of 930°C certainly promotes diffusion rates and facilitates the development of an almost ideal structure.

5. Conclusions

The $LiBH_4$–Mg_2NiH_4 composite shows some very interesting and unique properties. First, the two hydrides react mutually if the dehydrogenation of Mg_2NiH_4 is prevented by the application of a certain temperature dependant minimum hydrogen pressures. The restriction of the temperature during dehydrogenation was also proven to facilitate this concerted reaction: at 270 °C, i.e. below the melting point of $LiBH_4$, the reaction between solid $LiBH_4$ and Mg_2NiH_4 was observed. The mutual destabilization between these two compounds reduces the system's reaction enthalpy significantly. A value of about 13 kJ (mol H_2)$^{-1}$ was experimentally determined by evaluation of DSC analysis. In addition, a rather low entropy change of less than 70 J (K mol H_2)$^{-1}$ could be estimated. Furthermore, independent of the applied hydrogen pressure chosen for dehydrogenation, (almost) no $Li_2B_{12}H_{12}$ could be detected among the reaction products. As the dedicated experiment revealed, Mg_2Ni also reacts with $Li_2B_{12}H_{12}$ under formation of $MgNi_{2.5}B_2$. Hence, $Li_2B_{12}H_{12}$ can be regarded as an intermediate phase in the $LiBH_4$–Mg_2NiH_4 RHC and therefore, unlike the $LiBH_4$–MgH_2 system, no special dehydrogenation conditions (i.e. a certain minimum hydrogen pressure) need to be applied in order to preserve the system's hydrogen storage capacity. Interestingly, larger quantities of MgB_2 were identified in completely dehydrogenated $LiBH_4$–Mg_2NiH_4. Thermodynamic estimations suggest that the formation of MgB_2 is energetically less favourable than the intended reaction. However, this compound is formed via an accessible (side) reaction path between free magnesium and yet unreacted $LiBH_4$. It must be emphasized that the formation of MgB_2 does not impede reversibility. A high hydrogenation yield of approximately 90% was achieved after ten hydrogen cycles.

Acknowledgments

Supplementary materials

Supplementary material associated with this article can be found, in the online version, at doi:10.1016/j.jechem.2019.03.011.

References

[1] M. Paskevicius, L.H. Jepsen, P. Schouwink, R. Černý, D.B. Ravnsbæk, Y. Filinchuk, M. Dornheim, F. Besenbacherf, T.R. Jensen, Chem. Soc. Rev. 46 (2017) 1565–1634.
[2] J. Puszkiel, S. Garroni, C. Milanese, F. Gennari, T. Klassen, M. Dornheim, C. Pistidda, Inorganics 5 (2017) 74.
[3] S. Garroni, A. Santoru, H. Cao, M. Dornheim, T. Klassen, C. Milanese, F. Gennari, C. Pistidda, Energies 11 (2017) 1027.
[4] C. Milanese, S. Garroni, F. Gennari, A. Marini, T. Klassen, M. Dornheim, C. Pistidda, Metals 8 (2018) 567.
[5] S. Qiu, H. Chu, Y. Zou, C. Xiang, F. Xu, L. Sun, J. Mater. Chem. A 5 (2017) 25112–25130.
[6] A. Schneemann, J.L. White, S. Kang, S. Jeong, L.F. Wan, E.S. Cho, T.W. Heo, D. Prendergast, J.J. Urban, B.C. Wood, M.D. Allendorf, V. Stavila, Chemical Reviews 118 (2018) 10775–10839.
[7] Y. Nakamori, K. Miwa, H.W. Li, N. Ohba, S.-I. Towata, S.-I. Orimo, MRS Proc 971 (2006) 0971–Z02-01.
[8] Y. Nakamori, K. Miwa, A. Ninomiya, H.-W. Li, N. Ohba, S. Towata, A. Züttel, S. Orimo, Phys. Rev. B 74 (2006) 045126.
[9] L.H. Rude, T.K. Nielsen, D.B. Ravnsbaek, U. Boesenberg, M.B. Ley, B. Richter, L.M. Arnbjerg, M. Dornheim, Y. Filinchuk, F. Besenbacher, T.R. Jensen, Phys. Status Solidi A 208 (2011) 1754–1773.
[10] J.J. Reilly, R.H. Wiswall, Inorg Chem. 7 (1968) 2254–2256.
[11] Y.W. Cho, J.-H. Shim, B.-J. Lee, Thermal destabilization of binary and complex metal hydrides by chemical reaction: a thermodynamic analysis, in: Z.-K. Liu (Ed.), Calphad: Computer Coupling of Phase Diagrams and Thermochemistry, Elsevier, Netherlands, 2006, pp. 65–69.
[12] X.-D. Kang, P. Wang, L.-P. Ma, H.-M. Cheng, Appl. Phys. A 89 (2007) 963–966.
[13] J. Yang, A. Sudik, C. Wolverton, J. Phys. Chem. C 111 (2007) 19134–19140.
[14] A.-L. Chaudhary, G. Li, M. Matsuo, S.-I. Orimo, S. Deledda, M.H. Sørby, B.C. Hauback, C. Pistidda, T. Klassen, M. Dornheim, Appl. Phys. Lett. 107 (2015) 073905.
[15] P. Chen, Z. Xiong, J. Luo, J. Lin, K.L. Tan, Nature 420 (2002) 302–304.
[16] G. Barkhordarian, T. Klassen, R. Bormann, Patent: German Pub. No:DE1022004/061286 (2004).
[17] G. Barkhordarian, T. Klassen, M. Dornheim, R. Bormann, J. Alloys Compd. 440 (2007) L18–L21.
[18] J.J. Vajo, W. Li, P. Liu, Chem. Comm. 46 (2010) 6687–6689.
[19] G. Barkhordarian, T.R. Jensen, S. Doppiu, U. Bösenberg, A. Borgschulte, R. Gremaud, Y. Cerenius, M. Dornheim, T. Klassen, R. Bormann, J. Phys. Chem. C 112 (2008) 2743 274.
[20] J. Jepsen, C. Milanese, A. Girella, G.A. Lozano, C. Pistidda, J.M. Bellosta von Colbe, A. Marini, T. Klassen, M. Dornheim, Int. J. Hydrog. Energy 38 (2013) 8357–8366.
[21] T.T. Le, C. Pistidda, J. Puszkiel, M.V. Castro Riglos, F. Karimi, J. Skibsted, S.P. GharibDoust, B. Richter, T. Emmler, C. Milanese, A. Santoru, H. Hoell, M. Krumrey, E. Gericke, E. Akiba, T.R. Jensen, T. Klassen, M. Dornheim, J. Phys. Chem. C 122 (2018) 7642–7655.
[22] J.J. Vajo, S.L. Skeith, F. Mertens, J. Phys. Chem. B 109 (2005) 3719–3722.
[23] U. Bösenberg, S. Doppiu, L. Mosegaard, G. Barkhordarian, N. Eigen, A. Borgschulte, T.R. Jensen, Y. Cerenius, O. Gutfleisch, T. Klassen, M. Dornheim, R. Bormann, Acta Mater. 55 (2007) 3951–3958.
[24] F.E. Pinkerton, M.S. Meyer, G.P. Meisner, M.P. Balogh, J.J. Vajo, J. Phys. Chem. C 111 (2007) 12881–12885.
[25] B. Ao, Z. Zhang, Y. He, Y. Zhao, Int. J. Hydrog. Energy 38 (2013) 16471–16476.
[26] Z. Gavra, M.H. Mintz, G. Kimmel, Z. Hadari, Inorg. Chem. 18 (1979) 3595–3597.
[27] J. Genossar, P.S. Rudman, J. Phys. Chem. Solids 42 (1981) 611–616.
[28] D. Noréus, P.-E. Werner, Mater. Res. Bull. 16 (1981) 199–206.
[29] J.J. Reilly Jr, R.H. Wiswall Jr, Inorg. Chem. 7 (1968) 2254–2256.
[30] K. Zeng, T. Klassen, W. Oelerich, R. Bormann, J. Alloys Compd. 283 (1999) 213–224.
[31] P. Zolliker, K. Yvon, C.H. Baerlocher, JLCM 115 (1986) 65–78.
[32] W. Li, J.J. Vajo, R.W. Cumberland, P. Liu, S.-J. Hwang, C. Kim, R.C. Bowman Jr, J. Phys. Chem. Lett. 1 (2010) 69–72.
[33] K.J. Gross, A. Züttel, L. Schlapbach, J. Alloys Compd. 274 (1998) 239–247.
[34] W. Jung, Z. Naturforsch B 32 (1977) 1371–1374.
[35] P. Manfrinetti, M. Pani, S.K. Dhar, R. Kulkarni, J. Alloys Compd. 428 (2007) 94–98.
[36] U. Bösenberg, C. Pistidda, M. Tolkiehn, N. Busch, I. Saldan, K. Suarez-Alcantara, A. Arendarska, T. Klassen, M. Dornheim, Int. J. Hydrog. Energy 39 (2014) 9899–9903.
[37] B.R.S. Hansen, K.T. Møller, M. Paskevicius, A.-C. Dippel, P. Walter, C.J. Webb, C. Pistidda, N. Bergemann, M. Dornheim, T. Klassen, J.-E. Jørgensen, T.R. Jensen, J. Appl. Cryst. 48 (2015) 1234–1241.
[38] A.P. Hammersley, ESRF Internal Report ESRF97HA02T (1997).
[39] A.P. Hammersley, S.O. Svensson, M. Hanfland, A.N. Fitch, D. Hausermann, High Pressure Res. 14 (1996) 235–248.
[40] L. Lutterotti, in: Proceedings of the EMRS 2009 Spring Meeting - Symposium R, 268, 2010, pp. 334–340.

[41] L. Lutterotti, MAUD – Materials Analysis Using Diffraction. http://maud.radiographema.eu/ (visited on 19/10/2017).

[42] A. Züttel, S. Rentsch, P. Fischer, P. Wenger, P. Sudan, P. Mauron, C. Emmenegger, J. Alloys Compd. 356-357 (2003) 515–520.

[43] Y. Filinchuk, D. Chernyshov, R. Cerny, J. Phys. Chem. C 111 (2008) 10579–10584.

[44] M.R. Hansen, T. Vosegaard, H.J. Jakobsen, J. Skibsted, J. Phys. Chem. A 108 (2004) 586–594.

[45] B.V. Padlyak, N.A. Sergeev, M. Olszewski, V.T. Adamiv, Y.V. Burak, Phys. Chem. Glasses - B 55 (2014) 25–33.

[46] N. Bergemann, C. Pistidda, C. Milanese, T. Emmler, F. Karimi, A.-L. Chaudhary, M.R. Chierotti, T. Klassen, M. Dornheim, ChemComm 52 (2016) 4836–4839.

[47] N. Bergemann, C. Pistidda, C. Milanese, M. Aramini, S. Huotari, P. Nolis, A. Santoru, M.R. Chierotti, A.-L. Chaudhary, M.D. Baró, T. Klassen, M. Dornheim, J. Mater. Chem. A 6 (2018) 17929–17946, doi:10.1039/C8TA04748K.

[48] M. Matsuo, Y. Nakamori, S. Orimo, H. Maekawa, H. Takamura, Appl. Phys. Lett. 91 (2007) 224103.

[49] M. Paskevicius, M.B. Ley, D.A. Sheppard, T.R. Jensen, C.E. Buckley, Phys. Chem. Chem. Phys. 15 (2013) 19774–19789.

[50] H.I. Schlesinger, H.C. Brown, J. Am. Chem. Soc. 62 (1940) 3429–3435.

[51] M. Dornheim, S. Doppiu, G. Barkhordarian, U. Boesenberg, T. Klassen, O. Gutfleisch, R. Bormann, Scripta Mater. 56 (2007) 841–846.

[52] J.F. Stampfer Jr, C.E. Holley Jr, J.F. Suttle, J. Am. Chem. Soc. 82 (1960) 3504–3508.

[53] H. Hemmes, A. Driessen, R. Griessen, J. Phys. Condens. Matter. 19 (1986) 3571–3585.

[54] P. Martelli, R. Caputo, A. Remhof, P. Mauron, A. Borgschulte, A Züttel, J. Phys. Chem. C 114 (2010) 7173–7177.

[55] NIST Chemistry Webbook, https://down.nist.gov/

[56] T.E.C. Price, D.M. Grant, I. Telepeni, X.B. Yu, G.S. Walker, J. Alloys Compd. 472 (2009) 559–564.

[57] G. Afonso, A. Bonakdarpour, D.P. Wilkinson, J. Phys. Chem. C 117 (2013) 21105–21111.

[58] R.D. Shannon, Acta Cryst. A 32 (1976) 751–767.